Chemical Geology 527 (xxxx) xxxx

Contents lists available at ScienceDirect

Chemical Geology

journal homepage: www.elsevier.com/locate/chemgeo

Temperature and CO_2 dependency of global carbonate weathering fluxes – Implications for future carbonate weathering research

G. Romero-Mujalli*, J. Hartmann, J. Börker

Institut für Geologie, Centrum für Erdsystemforschung und Nachhaltigkeit (CEN), Universität Hamburg, Bundesstraße 55, 20146 Hamburg, Germany

ARTICLE INFO

Editor: Michael E. Böttcher

Keywords:
Carbonate system
Partial pressure of CO_2
Carbon cycle
Global model

ABSTRACT

Carbonate weathering and transfer of carbon towards the coastal zone is one of the relevant sinks for atmospheric CO_2, controlled by hydrology, ecosystem respiration, river water degassing, and further factors. Specifically, the connection between the soil-rock system to the river systems and instream processes affecting the weathering product fluxes remain under-researched. Based on constraints for soil-rock PCO_2, river PCO_2, and an identified dependence of river alkalinity on temperature, this work tested which controls should be considered at the global scale to accomplish a more holistic carbonate rock weathering model. Compiled river data suggests that with increasing land temperature, above approximately 11 °C, the amount of instream alkalinity in carbonate catchments decreases due to the temperature effect on the carbonate system, while the converse holds true at lower temperatures. Latter is in accordance with calcite dissolution controlled by soil-rock PCO_2 estimates based on ecosystem respiration. In addition, the type of the weathering system (open, semi-closed to closed system with respect to CO_2) was identified to be highly relevant for global weathering estimations. Open systems seem to be the most dominant boundary condition of calcite weathering in the soil profile. Tropical areas with thick soil layers, however, cause the carbonate weathering system to shift from open to semi-closed or closed system conditions. The findings support that calcite weathering fluxes in the soil profile are higher than the fluxes to the ocean transported by rivers. Furthermore, an increase in mean land temperature does not necessarily translate into an increase of lateral weathering fluxes because it might have an influence on soil development, discharge, CO_2 degassing, soil respiration and calcite dissolution. All these named factors need to be addressed to be able to quantify global carbonate weathering fluxes and to assess the sensitivity of carbonate weathering fluxes on climate variability. Future works should focus on collecting more temporal river chemistry data, mainly in tropical regions, to understand the main mechanism causing the observed decrease of alkalinity concentration with temperature.

1. Introduction

Chemical weathering is a key component of the processes transferring chemical species from the continents to the oceans (Berner et al. 1983; Kempe 1979a; Mackenzie and Garrels 1966; Walker et al. 1981). Numerous studies have shown that continental weathering is sensitive to environmental parameters (e.g. temperature, hydrology and vegetation) for a large variety of temporal scales (Calmels et al. 2014; Egli et al. 2008; Norton et al. 2014; White and Blum 1995). Specifically, the weathering of carbonate minerals, one of the most abundant minerals at the Earth surface (Hartmann et al. 2012; Hartmann and Moosdorf 2012), shows the highest weathering rates besides evaporites in comparison to most abundant lithological classes (Amiotte-Suchet and Probst 1993; Amiotte-Suchet and Probst 1995; Bluth and Kump 1994; Moosdorf et al. 2011). Carbonate weathering does not act as a sink for atmospheric CO_2 over geological timescales (Arvidson et al. 2006; Berner et al. 1983; Kempe 1979b). It impacts, however, the distribution of carbon between ocean and atmosphere at timescales below the mixing time of the ocean, shorter than 10^5 years (Berner and Berner 2012; Martin 2017). Although mapped sedimentary carbonate rocks cover only 10 to 14% of the terrestrial surface, excluding the area of ice shields (Dürr et al. 2005; Hartmann and Moosdorf 2012), carbonate rock weathering contributes about 50% to 60% to the dissolved products from rock weathering (Gaillardet et al. 1999; Meybeck 1987). This high proportion is because non-carbonate dominated lithological classes like mixed sediments, siliciclastic sediments, metamorphic rocks and felsic intrusive rocks contribute to carbonate weathering fluxes in addition (Hartmann et al. 2014b). Moreover, it had been estimated that

* Corresponding author.
E-mail address: gibran.romero.mujalli@uni-hamburg.de (G. Romero-Mujalli).

https://doi.org/10.1016/j.chemgeo.2018.08.010
Received 6 November 2017; Received in revised form 2 July 2018; Accepted 12 August 2018
0009-2541/ © 2018 The Authors. Published by Elsevier B.V. This is an open access article under the CC BY-NC-ND license (http://creativecommons.org/licenses/BY-NC-ND/4.0/).

carbonate weathering might be responsible for 34% to 50% of the global CO_2 consumption at short time scales (Gaillardet et al. 1999; Hartmann et al. 2009). One of the key processes controlling carbonate weathering flux in carbonate dominated lithologies is the partial pressure of CO_2 (PCO_2) in the soil (Calmels et al. 2014). In this system, organisms play an important role for weathering through the soil profile, concentrating the CO_2 and organic acids and providing more protons for weathering reactions (Kuzyakov 2006).

In the past, research on global land-ocean carbonate weathering fluxes focused on the rate of CO_2 uptake by chemical weathering at the global scale (Amiotte-Suchet and Probst 1995; Dupré et al. 2003; Hartmann et al. 2009; Hartmann et al. 2014b), applying functions based on empirical relationships with runoff, temperature, and soil properties (Amiotte-Suchet and Probst 1993; Bluth and Kump 1994; Hartmann et al. 2014b), while others have employed mechanistic models based on kinetic theory, chemical equilibrium and hydrological models, forced by ecosystem numerical models (Beaulieu et al. 2012; Goddéris et al. 2013; Goddéris et al. 2006; Roelandt et al. 2010). Although both types of model approaches aimed to calculate the total weathering flux to the ocean, and the CO_2 consumption by chemical reactions, the two approaches have significant differences. The functions based on observed relationships, phenomenological models, are the most simple and easy to apply in global calculations, e.g. in Earth system models (Goll et al. 2014). However, the principal disadvantage with the current phenomenological models is that generally a constant alkalinity concentration for carbonate weathering is assumed, independent of the temperature and soil-rock CO_2 concentration. Sometimes dilution effects for high runoff areas are addressed (Bluth and Kump 1994). On the other hand, the mechanistic models are often more computationally expensive and generally applicable at the local scale (Goddéris et al. 2006), and annual calculations for carbonate weathering are limited due to fast calcite dissolution, which force to decrease the time step for each calculation, while increasing significantly the computational time (Roland et al. 2013).

Furthermore, Gombert (2002) calculated the maximum carbonate dissolution by applying simplified equilibrium equations and a soil-rock PCO_2 function based on annual evapotranspiration from Brook et al. (1983). A soil-rock PCO_2 representation for the averaged conditions in the critical zone provides the ability to address the dynamics of weathering driven by ecosystem respiration. The advantage of using equilibrium equations over kinetics is that its numerical solution reduces the computational time, comparable to those of the application of phenomenological approaches in global weathering models. However, the applied PCO_2 equation based on annual evapotranspiration (Brook et al. 1983) in Gombert (2002) has some disadvantages for low temperature regions and may not address the role of soil water content enough, which is relevant for CO_2 production in the soil system (Romero-Mujalli et al. 2018).

Carbonate dissolution is a dynamic process and variations on timescale of hours are documented as well as fast precipitation depending mainly on the concentration of CO_2 in the aquatic system (Calmels et al. 2014; Pu et al. 2013; Roland et al. 2013; Serrano-Ortiz et al. 2010). Moreover, the kinetics of the reactions involved in carbonate dissolution are fast enough to reach equilibrium in 3 h in laboratory experiments (Dreybrodt et al. 1996; Reddy et al. 1981), implying that in the critical zone (soil-rock) the system could easily reach equilibrium with respect to a given PCO_2. Consequently, the concentration of carbonate weathering products in water leaving the soil-rock-system might be calculated based on equilibrium considerations using information on the soil-rock PCO_2 (Romero-Mujalli et al. 2018).

Pu et al. (2013) studied groundwater in karstic areas and they found that the water was always over-saturated with respect to calcite, and soil CO_2 production was driving seasonal hydrochemical variations in those waters. The highest PCO_2 in water occurred during the warm season. Moreover, Calmels et al. (2014) established that the chemical weathering gradient observed in the Jura Mountains can be explained by spatial variations in the amount of CO_2 in soils. The CO_2 in soils is produced by a combination of different processes, which include microbial activity, root respiration and dissolution of carbonate by acids (Edwards et al. 1973; Kuzyakov 2006; Li et al. 2008; Wang et al. 2015).

Difficulties while modelling global carbonate weathering may arise because: (i) often only calcite dissolution is considered, excluding other minerals that influence weathering fluxes (Gombert 2002); (ii) global approaches do not account for carbonate weathering influenced by strong acids, like sulphuric acid, in general (Beaulieu et al. 2011; Calmels et al. 2007; Calmels et al. 2014; Hercod et al. 1998; Spence and Telmer 2005; Torres et al. 2017); (iii) runoff based functions do not account for differences in soil-rock PCO_2 and temperature (Amiotte-Suchet and Probst 1995; Bluth and Kump 1994; Hartmann et al. 2014b); and, (iv) anthropogenic perturbations are not accounted in global carbonate weathering models, where application of fertilizers might impact CO_2 consumption by carbonate weathering (Perrin et al. 2008; Semhi et al. 2000).

In order to overcome such limitations and to better understand the role of the carbonate weathering in the Earth system, a set of approaches is compared and evaluated using river chemical data for catchments dominated by calcite dissolution. Approaches used are based on a river alkalinity parameterization (phenomenological approach) and equilibrium equations (mechanistic approach) to calculate the chemical weathering fluxes due to calcite dissolution from carbonate rocks, utilizing different constraining functions to estimate an annually representative partial pressure of CO_2 in the soil-rock system. The influence of additional minerals like sulphides and evaporites on generated alkalinity and calcium concentration is in further discussed, together with the question how does the abundance of open, semi-closed or closed system conditions with respect to soil CO_2 affect the generation of alkalinity fluxes.

2. Methods

2.1. Hydrochemical database

In order to evaluate calcite weathering fluxes to achieve the named objectives, the Global River Chemistry database (GLORICH) was used (Hartmann et al. 2014a), which combines hydrochemical data with catchment properties and characteristics. The GLORICH database represents over 17,000 sample stations, therefore, a data selection was an imperative step in this work to be able to study only sample stations with a dominant influence from calcite dissolution. A total of 299 sample locations were considered, representing 1798 single samples (Fig. 1). The selection was established for idealized conditions of calcite weathering. The following criteria needed to be fulfilled (Gaillardet et al. 2018; Romero-Mujalli et al. 2018):

(i) Samples with $[Ca^{2+}]/[SO_4{}^{2-}]$ molar ratios larger than 10 were selected to avoid relevant contribution from pyrite oxidation and sulphate minerals dissolution.
(ii) In order to minimize the effect of evaporite dissolution and silicate weathering, samples with $[Ca^{2+}]/[Na^{+}]$ molar ratios larger than 10 were selected, based on Gaillardet et al. (1999) relations and data analysis.
(iii) Water samples with $[Cl^{-}]/[Na^{+}]$ molar ratio < 2 were selected to minimize possible anthropogenic input.
(iv) $[Ca^{2+}]/[Mg^{2+}]$ molar ratio should be higher than 2 in water samples, to minimize contribution of other carbonate minerals besides calcite and to exclude further contribution of weathering of silicate minerals.
(v) Water samples with charge balance error (CBE) $< 10\%$ were chosen, to exclude samples with high uncertainty in reported concentrations.

A correction for rainwater contribution was not possible to apply

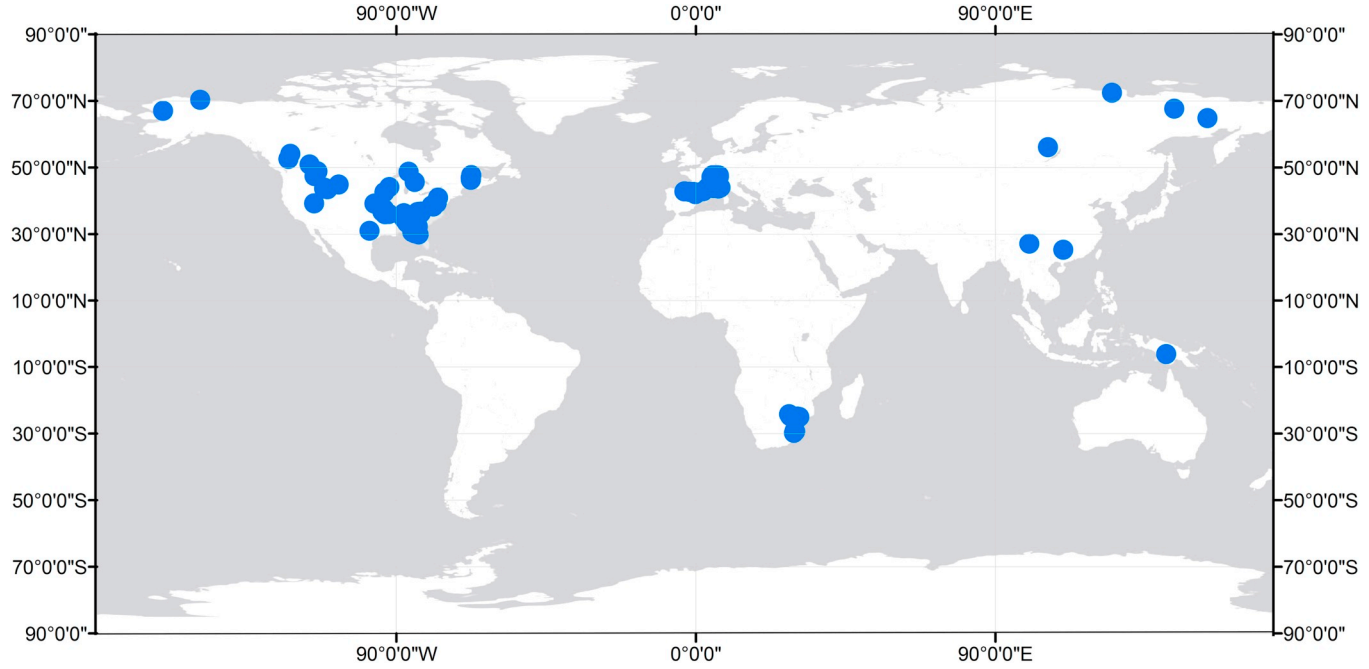

Fig. 1. Global localization of the 299 selected GLORICH sample stations after applying conditions described in Section 2.1. A total of 1798 single measurements are represented.

due to lack of knowledge of the contribution from local rainwater chemistry and dissolution of minerals other than calcite for each sampling location.

2.2. Alkalinity and PCO_2 parameterizations

In order to study controls on the river weathering fluxes from calcite dissolution, different approaches to estimate alkalinity were chosen (Table 1): (i) alkalinity was parameterized using a phenomenological approach and considers the observed alkalinity concentration dependence on temperature, which has a boomerang-shaped curve; and (ii) alkalinity was calculated by equilibrium calculations with a given PCO_2 and saturation index with respect to calcite (SIc; see Appendix A for details about thermodynamic calculations).

2.2.1. River alkalinity parameterization

The boomerang-shaped curve of alkalinity concentration in dependence of mean surface temperature identified for global rivers dominated by carbonate dissolution (Gaillardet et al. 2018) was used to represent carbonate weathering (hereafter as *river_alk*). Alkalinity was parameterized using annual land surface temperature of a catchment and implementing the non-linear Levenberg-Marquardt algorithm for the following function:

$$\log_{10} river_{alk} = (e^{b_1+b_2T+b_3T^2}), \quad (1)$$

"*river_alk*" is alkalinity in meq L^{-1}, T is mean annual land temperature (°C). The final parameters b_1, b_2 and b_3 were determined by sampling for each station 1000 times a random value based on mean values and standard deviation for reported alkalinity and temperature (Fig. 2) and subsequently estimating each time the b-parameters. The mean and standard deviation of b_1, b_2 and b_3 are -1.73 ± 0.08, 0.28 ± 0.02 and -0.0157 ± 0.0009, respectively. The standard deviation of Eq. (1) based on residuals analysis is 0.2 (logarithm of meq L^{-1}) for the 90% confidence level of the fitted function.

Table 1
Summary of the different settings implemented in this work to calculate global calcite weathering fluxes in rivers and from the soil-rock system at equilibrium with a specific calcite saturation index (SIc).

Nr.	Abbreviation	Estimate	Function	System	SIc	Reference
1	*CO_2atm*	PCO_2	0.000398 atm	Control	0	–
2	*river_alk*	Alkalinity	Eq. (1)	River	0	This study
3	*river_CO_2*	PCO_2	Global data	River	0 and 0.5	Lauerwald et al. (2015)
4	*soil_aet_CO_2*	PCO_2	Eq. (2)	Soil-rock	0	Brook et al. (1983)
5	*soil_tw_CO_2*	PCO_2	Eq. (3)	Soil-rock	0	Romero-Mujalli et al. (2018)

2.2.2. PCO_2 parameterizations

Different estimates for PCO_2 were applied as constraints to calculate alkalinity and calcium concentrations from calcite dissolution in equilibrium with a given PCO_2, either for the soil-rock system or within rivers

(1) Atmospheric PCO_2 (hereafter as *CO_2atm*) with a value of 0.000398 atm was used as a minimum threshold for aquatic PCO_2 which is at equilibrium with the carbonate system and representing a minimum baseline for carbonate weathering for comparison.
(2) Modelled global river water PCO_2 data after Lauerwald et al. (2015) was used to calculate concentrations of chemical species in equilibrium with calcite, assuming that this river CO_2 is derived from the soil-rock system and caused observed alkalinity concentrations in rivers. The possibility of CO_2 outgassing and secondary calcite precipitation in river will be discussed below. The applied river PCO_2 data represents global spatially-explicit estimates of river and stream PCO_2 for surface water stream orders of three and higher (hereafter as *global_river_CO_2*). Saturation indices with respect to calcite of 0 and 0.5 were considered to calculate concentrations of chemical species in rivers. The SIc = 0.5 was chosen based on an analysis of the filtered data and is close to the median SIc.
(3) Soil PCO_2 was calculated after Brook et al. (1983) (hereafter as *soil_aet_CO_2*). This equation depends only on the variables annual evapotranspiration (AET) and atmospheric PCO_2 (*CO_2atm*). The

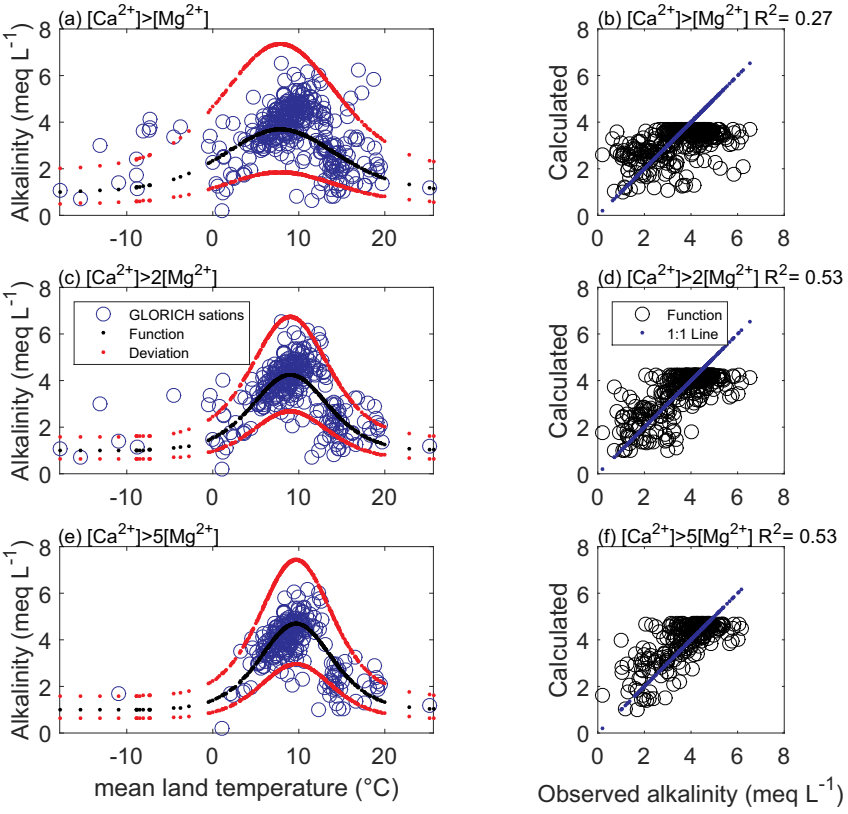

Fig. 2. Effect of magnesium on the construction of the function (Eq. (1)) for: (a) and (b) condition of $[Ca^{2+}]/[Mg^{2+}] > 1$; (c) and (d) condition of $[Ca^{2+}]/[Mg^{2+}] > 2$; and, (e) and (f) condition of $[Ca^{2+}]/[Mg^{2+}] > 5$. Plots (a), (c) and (d) are alkalinity (meq L^{-1}) against mean annual land temperature (°C); and (b), (d) and (f) scatterplots represent the relationship between calculated (Eq. (1)) and observed alkalinity. Given alkalinity are the mean per sampling location, using 299 catchments.

equation (Eq. (2)) was originally constructed using soil PCO_2 data from 19 locations at different depths, and is defined as:

$$\log_{10}(soil\_aet\_CO_2) = \log_{10}(PCO_2 atm) + 2.09(1 - e^{-0.00172AET}), \quad (2)$$

(4) In addition, the function for estimating soil PCO_2 after Romero-Mujalli et al. (2018) was applied (hereafter as *soil_tw_CO₂*) to calculate the concentration of chemical species at equilibrium with calcite. Parameters for the equation (Eq. (3)) were derived using the Levenberg-Marquardt algorithm for non-linear methods. This equation uses land surface temperature and soil volumetric water content as the main predictor variables for estimating an averaged soil-rock PCO_2.

$$\log_{10}(soil_{tw_{CO_2}}) = \frac{e^{\left(b_1\theta + \frac{b_2}{\theta}\right)}}{(b_3 + e^{b_4 T})} + \log_{10}(PCO_2 atm), \quad (3)$$

where T is temperature in °C, θ represents the soil volumetric water content ($m^3\,m^{-3}$), $CO_2 atm$ is the partial pressure of CO_2 (atm) in the atmosphere, and in this work a value of 0.000398 was considered. Fitted parameters b_1, b_2, b_3 and b_4 have values of −3.0, −0.25, 0.09 and − 0.34, respectively. The calculated standard deviation for this function is 0.6 ($\log_{10}PCO_2$).

2.3. Global chemical weathering calculations

Global information in gridded format (Section 2.4) was used to determine spatially-explicitly alkalinity or calcium concentration related to the dissolution of calcite and to calculate weathering rates either from the soil-rock system or in rivers (Fig. B.1). The weathering rates are calculated by the following equation:

$$r = C_i * q, \quad (4)$$

where, r is the alkalinity weathering rate expressed in mmol of C_i m^{-2} a^{-1}, C_i is the concentration of a chemical species produced by calcite dissolution (calculated as explained in Section 2.2) in mmol m^{-3} (or meq m^{-3}), and q is the surface runoff in $m^3\,m^{-2}\,a^{-1}$. The alkalinity rate represents the rate of different chemical species (C_i is representing here $[HCO_3^-] + 2[CO_3^{2-}] + [OH^-] - [H^+]$).

The global alkalinity weathering flux (F_t) is calculated by the following equation:

$$F_t = \sum_{k=1}^{n} r_k A_k, \quad (5)$$

where A is the area of carbonate sedimentary rocks (SC) in m^2, subscript k stands for specific grid-cell, and n is the total number of grids in the map. Global weathering flux can be translated to CO_2 consumption (mol C a^{-1}) by using the stoichiometric relations (Eq. (A.13)), where mole of CO_2 consumed is equivalent to mole of Ca^{2+} in solution.

The obtained alkalinity rates were compared with approaches applying two runoff based phenomenological models (Amiotte-Suchet and Probst 1995; Bluth and Kump 1994).

Amiotte-Suchet and Probst (1995) calculate alkalinity rates depending on runoff by:

$$r_{SP} = 3.1692 * q, \quad (6)$$

where r_{sp} is the alkalinity rate in meq alkalinity $m^{-2}\,a^{-1}$ and q is the runoff in $mm^3\,mm^{-2}\,a^{-1}$. This approach considers a constant alkalinity concentration.

The equation from Bluth and Kump (1994) is defined as:

$$r_{BK} = \frac{10^{4.521}(0.1 * q)^{0.934}}{1000}, \quad (7)$$

where r_{BK} is the alkalinity rate in meq alkalinity $m^{-2}\,a^{-1}$. Eq. (7) considers a small dilution effect for high runoff values.

2.4. Global datasets

The applied global runoff dataset (Fekete et al. 2002) combines observed river discharge information with a water balance model to increase accuracy. The calculations were performed for areas with

sedimentary carbonate rocks (SC) as mapped in the GLIM database (Hartmann and Moosdorf 2012). The global mean annual surface temperature was extracted from Hijmans et al. (2005). Global annual evapotranspiration (AET) in mm a^{-1} and the soil volumetric water content (θ) in $m^3 m^{-3}$ data from the Global Land Evaporation Amsterdam Model (GLEAMv3.0) were used, which consist of a set of algorithms that calculate the different components of terrestrial evaporation based on satellite observations (Martens et al. 2016; Miralles et al. 2011). Global calculations were performed implementing a global resolution of 20 km per grid cell.

3. Results

About half of the alkalinity from carbonate weathering represents the CO_2 sink due to weathering, applying the selection procedure for data used in the analysis (Section 2.1). Alkalinity is approximately equal to half the concentration of calcium plus magnesium. As in general only low magnesium concentrations relative to calcium are abundant in the selected samples, alkalinity is used to represent the dissolution of calcite in the further discussion. A detailed analysis of calcium concentrations in rivers and its relation to environmental factors is given in an accompanying publication (Gaillardet et al. 2018).

3.1. Temperature and magnesium dependency of river alkalinity

The identified alkalinity concentration in rivers dominated by dissolution of calcium carbonates can be described by a Gaussian function in dependence of land surface temperature (Fig. 2). The highest alkalinity concentration is found for temperate climate conditions with a land surface temperature of approximately 11 °C.

The used alkalinity approach (Eq. (1)) is applicable to represent the general temperature dependency of calcite dissolution products found in rivers. However, the presented mean function has a relatively high uncertainty as marked by the red lines due to the large scattering of the mean alkalinity data (Fig. 2).

If different selection criteria for the Ca^{2+}/Mg^{2+} molar ratio are used, the effect of Mg^{2+} concentration on the observed scattering of alkalinity becomes evident (Fig. 2). Controls on dissolution processes of abundant magnesium rich minerals, like dolomite or silicates, and possibly effects on in-stream carbonate precipitation, produce a different alkalinity pattern than the one indicated by the dissolution of calcite. Choosing water samples with a lower relative magnesium concentration ($[Ca^{2+}] > 2[Mg^{2+}]$ and $[Ca^{2+}] > 5[Mg^{2+}]$) results in a better relationship between calculated and observed mean values for alkalinity, and a tighter boomerang-shaped curve (Fig. 2c–f), than water samples with relatively high Mg^{2+} concentration (Fig. 2a–b). The best fit for (Fig. 2c) the case $[Ca^{2+}] > 2[Mg^{2+}]$ is used in further to describe the observed behaviour of alkalinity in dependence on temperature.

3.2. Temperature and CO_2 control on dissolution of calcite

Applying thermodynamic equations for the system $CaCO_3$-CO_2-H_2O suggest that at constant PCO_2 the concentration of dissolved calcite is indirectly proportional to temperature. Hence, calculated alkalinity reproduces this behaviour when a constant atmospheric CO_2 of 0.000398 atm is considered as a baseline scenario for the discussion (*CO_2atm* setting; Fig. 3f).

Applying different PCO_2 scenario constraints to calculate river alkalinity due calcite dissolution (scenarios: estimated river PCO_2, Fig. 3b; PCO_2 estimated by annual evapotranspiration, Fig. 3c; or PCO_2 estimated by surface land temperature and soil water content Fig. 3d) does not reproduce the observed alkalinity dependency on temperature based on observations (Fig. 3a and e) for the given temperature range.

The closest pattern to the observed alkalinity is the approach using temperature and soil water content to estimate an average soil-rock-PCO_2 (*soil_tw_CO_2*; Fig. 3c). For this approach chemical concentrations from calcite dissolution are calculated before the water discharges into rivers, because this approach was derived based on spring water samples in karst areas (Romero-Mujalli et al. 2018). However, the estimated alkalinity in high temperature regions (> 12 °C) is on average for the *soil_tw_CO_2* approach (green line in Fig. 3c) higher than the observed mean alkalinity values from the GLORICH database (Fig. 3e) or the predicted ones by the boomerang-shaped alkalinity function, based on a temperature dependency (Fig. 3a). This might be because the *soil_tw_CO_2* approach predicts the production of alkalinity in the soil-rock system by design and does not consider other relevant processes affecting the $CaCO_3$-CO_2-H_2O system in the river, e.g. dilution in high runoff areas, CO_2 degassing and calcite precipitation in the river, or the existence of semi to closed system conditions with respect to soil PCO_2 (Bono et al. 2001; Lauerwald et al. 2015; van Geldern et al. 2015; Zhong et al., 2017).

The application of the PCO_2 estimation based on annual evapotranspiration for the soil-rock system (*soil_aet_CO_2*) or river PCO_2 (*river_CO_2*) are not replicating the observed river alkalinity pattern (Fig. 3e). Only a weak decreasing trend for elevated temperatures can be observed. The application of two different saturation indices for river PCO_2 (Fig. 3b) reveals no different calculated alkalinity pattern, considering the shape and trend, with exception of different resulting concentrations. Considering the applied thermodynamic equation systems for the scenarios in Fig. 3c to d, temperature does not represent the strongest direct control, but it influences the biological activity and hence the PCO_2 in the soil system.

3.3. Comparing estimated global weathering fluxes

The different approaches to estimate generated alkalinity concentrations causes for each grid point a different value in the global weathering calculation, and therefore aggregated global fluxes are different (Fig. 4). Calculated global calcite weathering fluxes are represented as CO_2 consumption fluxes in Fig. 4, comparing the different scenarios with previously used runoff-based functions or phenomenological equations, established by Amiotte-Suchet and Probst (1995) and Bluth and Kump (1994). These latter two approaches, often used in global studies to represent not only calcite but total carbonate weathering fluxes, produce higher global river alkalinity fluxes than the baseline calculation (using recent atmospheric PCO_2 as constraint), estimated river PCO_2 (using a calcite saturation index of 0) and the boomerang-shaped function for alkalinity, based on a temperature dependency (considering the mean of the calculations for *river_alk* scenario). The global estimates for the soil-rock system are only slightly higher on average compared to the results from Amiotte-Suchet and Probst (1995) and Bluth and Kump (1994). Two approaches, which allow uncertainty evaluations, show a significant span of possible global fluxes. Note that the estimates from the previous works were not used here, but new ones recalculated using a homogenized geodatabase to allow comparison of results (Fig. 4) for the process discussion below.

The calculated global chemical weathering fluxes are only related to areas with carbonate sedimentary rocks (labelled SC in the GLIM database), and do not represent fluxes from mixed sediment areas or trace carbonate fluxes from other lithological classes (Fig. 4). The calculated global fluxes from mapped carbonate sedimentary rocks are thus lower than total global carbonate weathering fluxes including further contributing lithologies. The total area of SC used in this work is 10.94×10^6 km^2, which is approximately 1% higher than in Hartmann et al. (2014b), but still 7% less than reported by the GLIM database (Hartmann and Moosdorf 2012). This is because the surface area was calculated from a vector format into a grid format.

Comparing calculated fluxes using the mean alkalinity per sampling station with runoff seems to justify the global application of the previous phenomenological models (Fig. 5a). However, the available data allow comparison only for a limited runoff range. Approaches using

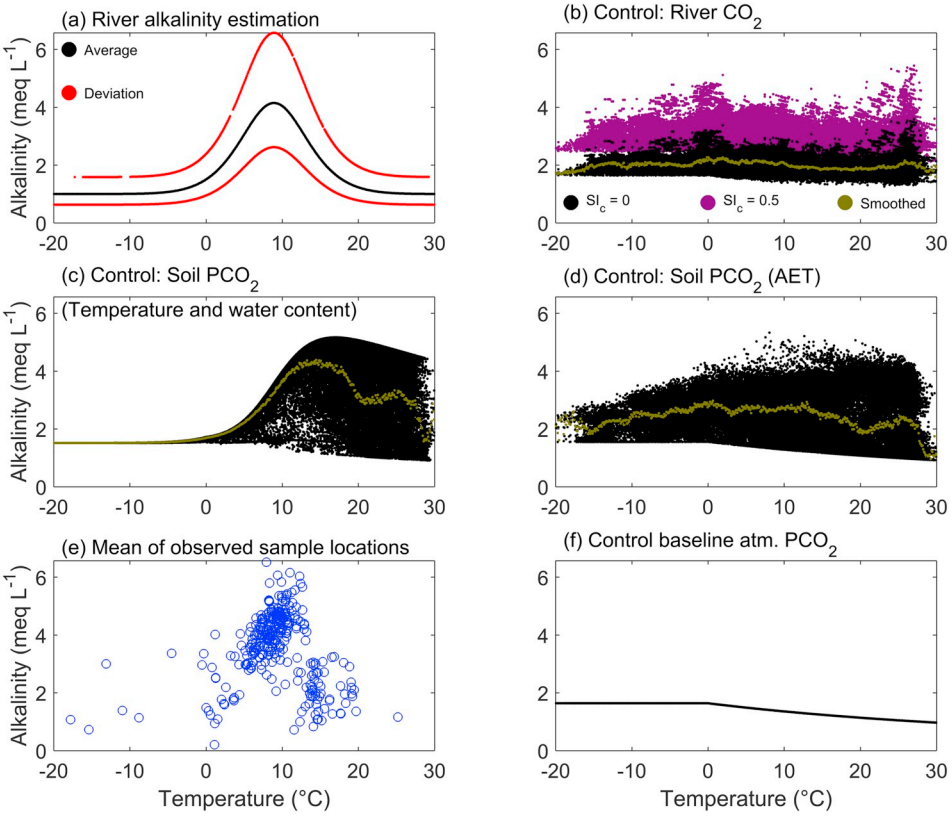

Fig. 3. Global spatially explicitly calculated alkalinity (meq L^{-1}) against average land temperature (°C) using a 20 km^2 grid cell definition for the scenarios river alkalinity-temperature function *river_alk* (a), and three PCO_2 estimates as constraint (b to d). For *river_PCO₂* (b) estimated river PCO_2 and the calcite saturation index (SIc) of 0 and 0.5 are used as constraint. To estimate the soil-rock PCO_2 the constraints temperature and soil water content were used in (c) (*soil_tw_CO₂*) and the annual evapotranspiration rate (AET) in (d) (*soil_aet_CO₂*). Each black point represents a calculation per 20 km^2 grid cell (Section 2.3). For comparison the reference mean values of alkalinity of selected GLORICH sample stations (e), and the baseline scenario using atmospheric PCO_2 as constraint (*CO₂atm*; f) are given. The red points in a) represent the deviation from the *river_alk* function, and the olive points in (b) to (d) represent the moving averages using a span value of 1 °C. The purple points in (b) are the calculated alkalinity values considering a SIc of 0.5, while black points represent the calculation for SIc = 0. (For interpretation of the references to colour in this figure legend, the reader is referred to the web version of this article.)

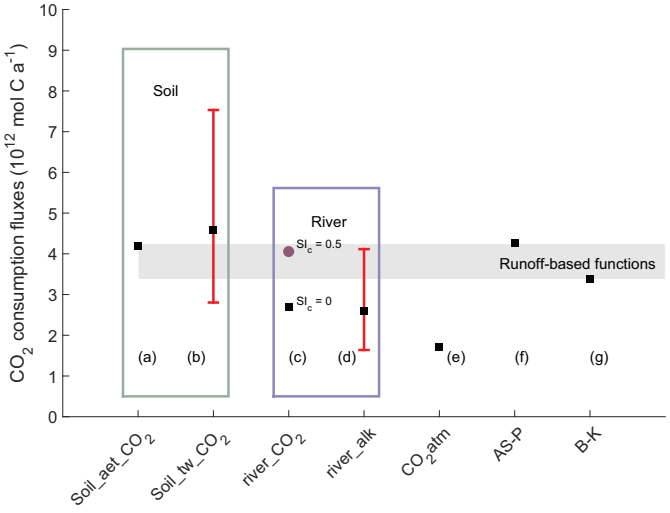

Fig. 4. Total CO_2 consumption fluxes (10^{12} mol C a^{-1}) due to CO_2 consumption by global calcite dissolution for different settings: (a) and (b) CO_2 fluxes due to calcite weathering in soil (*soil_aet_CO₂* and *soil_tw_CO₂* settings, respectively); (c) and (d) CO_2 fluxes using river settings (*river_CO₂* and *river_alk*, respectively); (e) considering the constant value of 0.000398 atm for atmospheric PCO_2 (*CO₂atm*); and, (f) and (g) previous runoff-based functions from Amiotte-Suchet and Probst (1995) and Bluth and Kump (1994), identified as AS-P (Eq. (6)) and B-K (Eq. (7)), respectively. The grey rectangle is the interval for previous phenomenological equations AS-P and B-K. Red lines are the maximum and minimum limits when considering deviation due to residuals for Eqs. (1) and (3). The purple circle represents the total carbon flux when a saturation index SIc = 0.5 is considered for the river PCO_2 estimate. (For interpretation of the references to colour in this figure legend, the reader is referred to the web version of this article.)

climate sensitive variables show considerable deviation from the phenomenological models, by approximately ± 50% in Fig. 5b to d, and lower deviation for the approach using estimated river PCO_2 as constraint (Fig. 5e). This is because the calculated alkalinity concentrations (C_i from Eq. (4)) vary with temperature, soil water content or evapotranspiration. A significant increase in alkalinity fluxes is calculated when the observed average river saturation index with respect to calcite (SIc) of 0.5 is considered (Fig. 7) using river PCO_2 as constraint (Fig. 4). This results in an increase of about 50% for calculated global fluxes, reaching a comparable global value than estimated by runoff-based functions in Fig. 4(AS-P & B-K).

The river PCO_2 data from Lauerwald et al. (2015) is based on climate sensitive parameters like air temperature, net primary productivity (NPP) and a geomorphological component, gradient of slope of a catchment. As this latter catchment property steers the degassing of CO_2 (Lauerwald et al. 2015), the river CO_2 constraining approach considers a factor directly addressing the potential to precipitate calcite in rivers, and thus lowering the alkalinity fluxes. However, it should be noted that the river PCO_2 estimation is valid only for stream orders larger than two (Lauerwald et al. 2015), and the considerable outgassing from rivers with smaller stream order was not captured here, due to lack of general knowledge in how to parameterized this for small streams at the global scale (Marx et al. 2017). This may in part contribute to the observable difference to the river alkalinity concentration based on observations (Fig. 3).

3.4. The influence of dilution on global calculations

A further simulation was carried out to study the effect of dilution for high runoff areas on global carbon fluxes and alkalinity rates, because it has been demonstrated that hydrology, besides ecosystem respiration, is a relevant control on the weathering rate from carbonate

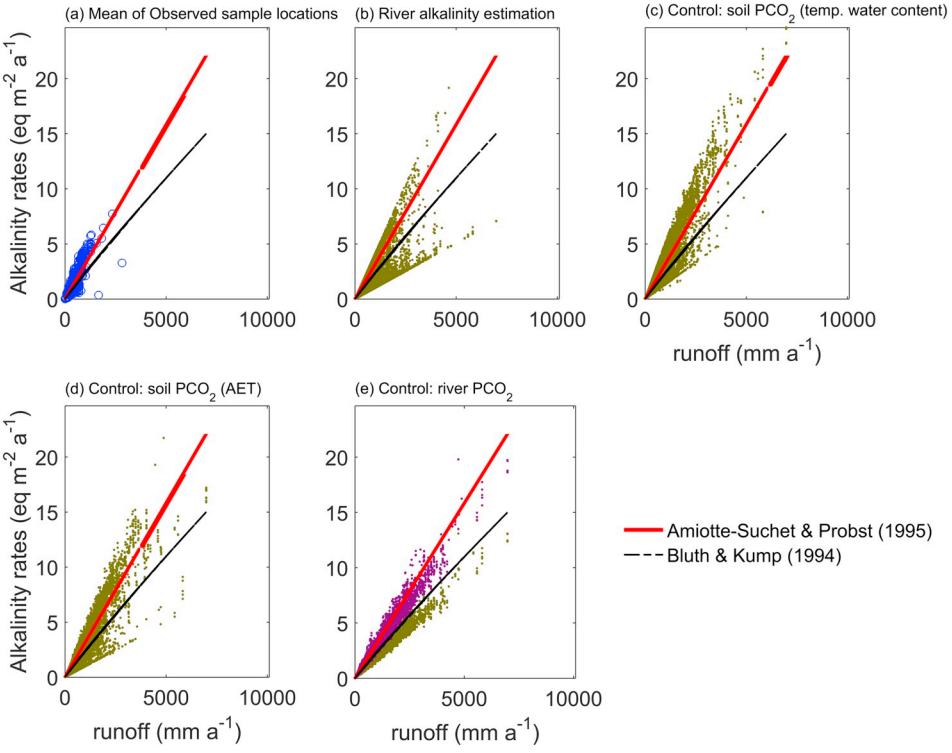

Fig. 5. Global alkalinity rates ($eq\,m^{-2}\,a^{-1}$) against runoff ($mm^3\,mm^{-2}\,a^{-1}$) calculated using (a) mean values of 299 sample stations in GLORICH database, (b) *river_alk*, (c) *soil_tw_CO₂*, (d) *soil_aet_CO₂*, and (e) *river_CO₂*. Previous phenomenological models based on runoff are represented by the red (Amiotte-Suchet and Probst 1995) and black lines (Bluth and Kump 1994), calculated using Eqs. (6) and (7), respectively. Note that c) and d) represent alkalinity rates generated in the soil-rock system, while the other approaches are based on river data. The purple points are the calculated alkalinity values considering a SIc of 0.5. (For interpretation of the references to colour in this figure legend, the reader is referred to the web version of this article.)

mineral dissolution in catchments (Zhong et al., 2017). At high runoff, calcite dissolution might not achieve equilibrium and the water will be undersaturated with respect to calcite, or a substantial amount of surface runoff not percolating into the ground is added to the river water. Due to the lack of instant discharge data for a sufficient number of catchments, a comparison with annual runoff is conducted to study first order patterns, which may emerge if dilution would be a relevant factor to be considered. Therefore, a correction coefficient as proposed by Bluth and Kump (1994) was used to calculate a dilution effect on concentrations of chemical species (C_i) with increasing runoff, expressed by the following equation:

$$C_i = \frac{C_{eq}}{q^{0.066}}, \tag{8}$$

where C_{eq} stands for the concentration of chemical species i ($mol\,L^{-1}$), calculated by equilibrium equations, and q is the runoff ($mm^3\,mm^{-2}\,a^{-1}$). The dilution parameter of "0.066" was taken from Bluth and Kump (1994) for catchments dominated by carbonate minerals because they have correlated alkalinity with runoff associated to carbonate rocks. Accordingly, a decrease in alkalinity rates for increasing runoff can be observed, as expected (Table 2). Nevertheless, this correction was not applied to the *river_alk* and *river_CO₂* settings because the dilution effect may be already imprinted into the river water composition. An application of the dilution effect would decrease global carbon fluxes significantly (−34% approximately, Table 2), similar to the approaches using river water composition as constraint (*river_alk* and *river_CO₂*). The scenarios with dilution effect result in lower global fluxes than the scenarios using parameterizations based on Bluth and Kump (1994) and Amiotte-Suchet and Probst (1995). A dilution effect based on annual data is hard to apply, as dilution should happen at the event scale during rainy periods, and would therefore demand a calibration for parameters using event scale data. However, the calculation suggests, that the chosen simple parameterization achieves a plausible effect towards the right direction. Further results discussed below on the open-versus closed system condition (Section 3.6) suggest that the dilution effect should be weaker, if using annual data as done here.

Table 2
Global CO_2 consumption fluxes associated to modelled calcite dissolution using different approaches based on phenomenological functions and equilibrium equations. The dilution effect was calculated for settings considering PCO_2 constraints for the soil-rock system and the baseline scenario by implementing Eq. (8).

Method-simulation setting	CO_2 consumption (10^{12} mol C a^{-1}). Without dilution effect	CO_2 consumption (10^{12} mol C a^{-1}). Including dilution effect (Eq. (8)).
Amiotte-Suchet and Probst (1995)	4.3	n.a.
Bluth and Kump (1994)	3.4	n.a.
soil_et_CO₂	4.3	2.8
soil_tw_CO₂	4.6 (2.8–7.6)	3.0 (1.8–4.9)
river_CO₂	2.7 (4.1[a])	n.a.
river_alk	2.6 (1.6–4.1)	n.a.[b]
CO₂atm	1.8	1.2

n.a.: not applicable.
[a] CO_2 fluxes calculated using SIc = 0.5.
[b] *river_alk* calculates directly the alkalinity based on relationship with temperature as described by Gaillardet et al. (2018), hence, it might reflect implicitly the dilution effect.

3.5. Modelled versus observed alkalinity

Comparing calculated alkalinity mobilization in the soil-rock system (*soil_tw_CO₂* and *soil_aet_CO₂*) with reported alkalinity values in rivers shows a better prediction potential, due resulting soil-rock PCO_2, for the approach using temperature and soil water content as constraint than evapotranspiration (*soil_tw_CO₂* and *soil_aet_CO₂*, respectively). Two different temperature intervals (≥ 11 °C and < 11 °C) are distinguished to address the maximum of alkalinity in the observed data (Fig. 2). The *soil_tw_CO₂* setting underestimates for the low temperature interval (blue points in Fig. 6a) observed values systematically by about 1 $meq\,L^{-1}$. For elevated temperatures the model tends to produce higher alkalinity values (red points in Fig. 6a). This might be in

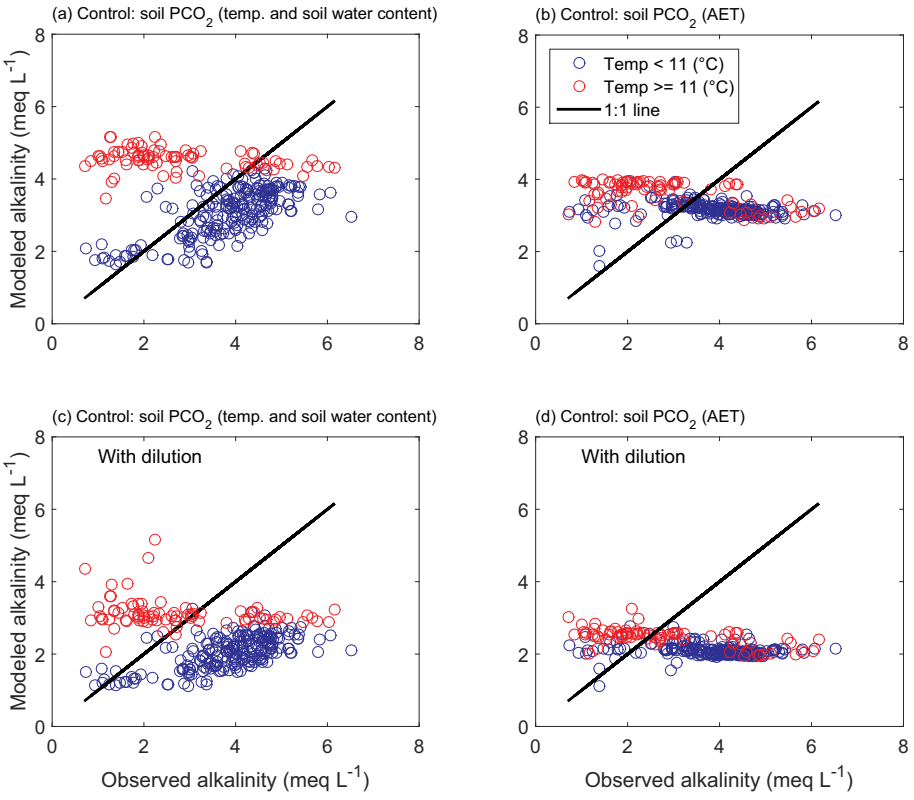

Fig. 6. Comparison between calculated and observed alkalinity using as a reference the mean values reported for the 299 selected sample stations (Fig. 1). (a) *soil_tw_CO2*, (b) *soil_aet_CO2*, (c) *soil_tw_CO2* including dilution, and (d) *soil_aet_CO2* applying dilution effect. Dilution was applied using Eq. (8). The black line represents the ideal 1:1 relationship, red circles are data with surface mean temperature higher or equal than 11 °C, and blue circles are data with surface mean temperature < 11 °C. (For interpretation of the references to colour in this figure legend, the reader is referred to the web version of this article.)

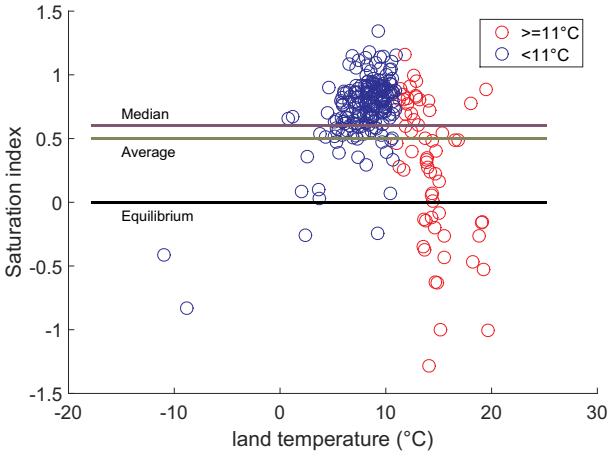

Fig. 7. Saturation index with respect to calcite (SIc) against mean annual land temperature (°C) for selected 299 GLORICH sample locations. The green line represents the average value, black line is the equilibrium condition (SIc = 0), purple line is the median value and red circles represent the relatively high temperature region (≥ 11 °C). (For interpretation of the references to colour in this figure legend, the reader is referred to the web version of this article.)

accordance with degassing of CO_2 and subsequent reduction of alkalinity in the river system. However, undersaturated conditions can be observed for some samples in this temperature region (Fig. 7). The relationship between modelled and observed values for elevated temperature regions does not improve when a dilution effect is considered, taking the 1:1 line as reference (Fig. 6c), and the tendency to underestimate reported values increases. Therefore, a further process, not represented in the model assumptions, might be responsible for overestimation in high temperature regions (see results for open and closed system conditions in the next section).

Calculated alkalinity values using evapotranspiration as constraint (*soil_aet_CO2*) shows no distinctive relationship with observed values in the GLORICH database, with and without considering a dilution effect (Fig. 6b and d, respectively). This indicates that the application of mean annual evapotranspiration to estimated soil-rock PCO_2 (Brook et al. 1983) is not the best selection, based on the data presented in this work. This might be due to the effect of considering different depths during the creation of this soil PCO_2 function (Eq. (2)), and due to measurements during growing seasons for low temperature regions, affecting the lower limit for mean annual soil PCO_2, were applied (Brook et al. 1983; Romero-Mujalli et al. 2018).

3.6. Transition from open to closed system condition with respect to soil-rock PCO_2

Calcite dissolution under closed conditions with respect to a given soil PCO_2 can generate low concentrations of calcium and alkalinity, causing a low saturation index with respect to calcite (SIc), as described by Thrailkill and Robl (1982). The closed conditions are achieved in areas where the water is isolated from the area of soil CO_2 production before reaching an equilibrium with calcite (Deines et al. 1974). Therefore, this condition is probably found in deeper regions of the soil-rock system, where water residence time in the unsaturated zone is less than the time required to reach equilibrium. A global soil depth database was used to evaluate if a systematic bias exists assuming open system conditions. Therefore, the ratio between modelled (using *soil_tw_CO2* setting) to observed alkalinity was plotted against reported soil depth. The ISRIC-WISE v3.0 soil database with a half degree resolution was used for this analysis. It is characterized by 45,948 unique soil map units, where parameters for each soil unit are estimated using a set of 9600 soil profiles (Batjes 2005). Extracted values from this database indicate that soils associated with calcite dissolution present, in general, a maximum soil depth < 2 m (average of 1 m). Calculated alkalinity concentration, under open conditions, using the best representation for soil PCO_2 found in this work (*soil_tw_CO2*, Section 3.5), was normalized to observed alkalinity values, and the ratio calculated/observed compared with soil depth for each sample location (Fig. 8).

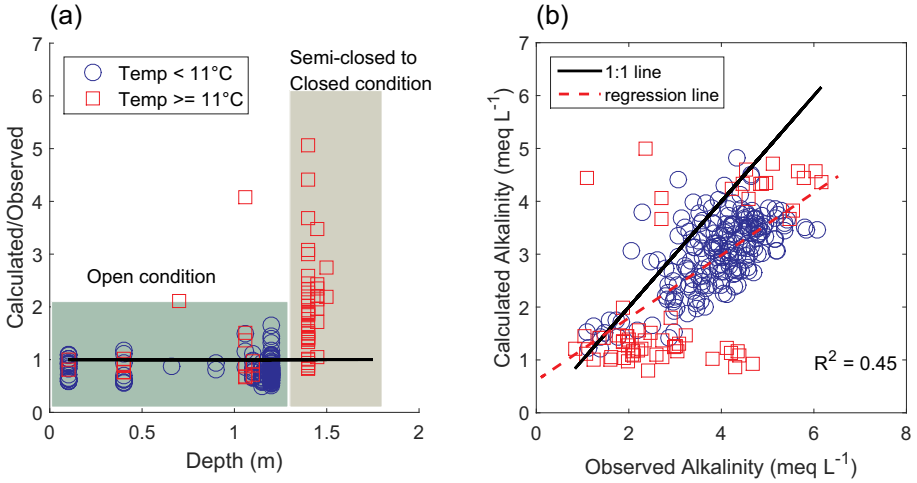

Fig. 8. Scatter plots showing: (a) alkalinity normalization (Calculated/Observed) against depth, based on ISRIC-WISE v3.0, considering open conditions with respect to CO_2; and (b) calculated against observed alkalinity when closed conditions with respect to CO_2 in deeper soils is included. Alkalinity was calculated using *soil_tw_CO2* setting (best fit suggested by Section 3.5) and compared with selected mean values of 299 GLORICH stations. The black line stands for the 1:1 relationship, the red line represents the linear regression with R^2 of 0.45. Shaded regions are the estimated system conditions. A depth of 1.3 m was established as the limit between open and closed conditions based on the increasing deviation. (For interpretation of the references to colour in this figure legend, the reader is referred to the web version of this article.)

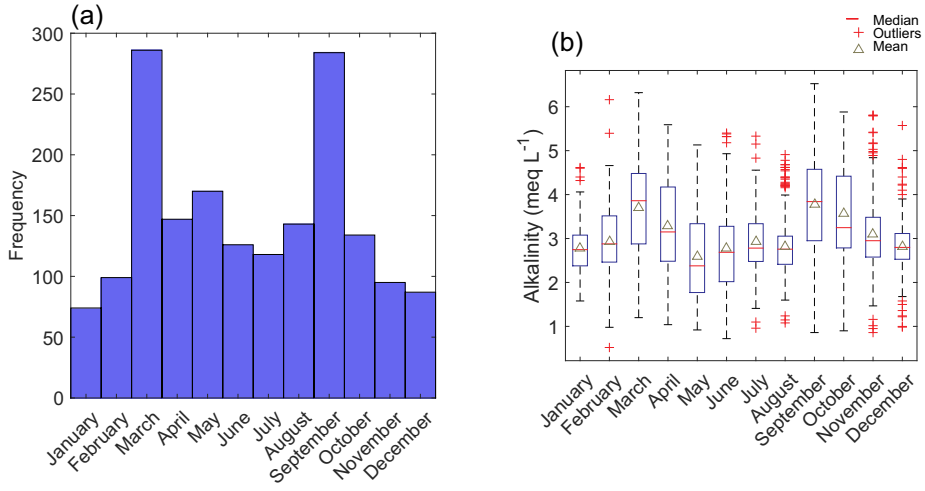

Fig. 9. Monthly data of 1798 single measurements from 299 GLORICH sample stations (Section 2.1). (a) Histogram of months sampled showing the preferential months; and, (b) box-plot of alkalinity grouped by months. Monthly data of 1798 single measurements from 299 sample stations.

Overestimation of calculated alkalinity considering open system conditions tends to increase with soil depths (Fig. 8a). This would be expected for a general pattern of a transition from open to closed system conditions with respect to soil CO_2.

To address the observation, alkalinity was newly calculated assuming open system conditions for soil depth < 1.3 m and closed system conditions for soil depth > 1.3 m. In theory, semi-closed conditions can be estimated, but for the purpose of showing the maximum effect, closed system conditions are chosen. Newly calculated alkalinity results in a better approximation compared to observations (Fig. 8b). Therefore, soil depth is a parameter that helps to identify conditions for the onset of the transition from open to closed system conditions. Nevertheless, the systematic tendency towards underestimation of river alkalinity using soil-rock PCO_2 estimation is still present. The shape of the scatter plot (Fig. 8b) indicates that a systematic bias for the applied *soil_tw_CO2* function exists. Further studies, applying a larger sample set to retrieve a *soil_tw_CO2* type function as used in Romero-Mujalli et al. (2018) or improving the soil PCO_2 estimate by including further factors, may lead in the future to better approximations.

If closed system conditions are assumed for locations with soil depths > 1.3 m the calculated global CO_2 consumption would decrease to 1.0×10^{12} mol C a^{-1} (applying *soil_tw_CO2*). This is less than the flux for open system conditions assuming that soil-rock PCO_2 is only equivalent to the atmosphere (*CO2atm*), with 1.8×10^{12} mol C a^{-1}. This result indicates that a transitional zone exists, and the simple two steps model used here is not sufficient for a global application. The calculation suggests that the spatial global abundance of closed system conditions with respect to soil CO_2 is limited. Results indicate that this transitional zone is preferentially abundant in high temperature regions, where thicker soils exist. A spatially-explicit knowledge of where, and under which conditions, the transition towards semi or even closed system conditions appears seems, therefore, a relevant research objective to constrain global carbonate weathering fluxes, specifically in the tropics.

However, the general pattern of river alkalinity can already be replicated with the existing parameterization of the *soil_tw_CO2* soil-rock PCO_2 function (using a limited available dataset for parameterization), and by using information of open-closed-system conditions. The relative systematic underestimation of river alkalinity by about 1 meq L^{-1} (Fig. 8b) would not allow for further degassing, which can be observed in the rivers (specifically for the temperature range < 11 °C). An improvement of the soil-rock-PCO_2 estimation needs to address this additional effect and would therefore need to produce higher soil-rock PCO_2 values as suggested by the deviation from the 1:1 line considering open-closed-system conditions in Fig. 8b.

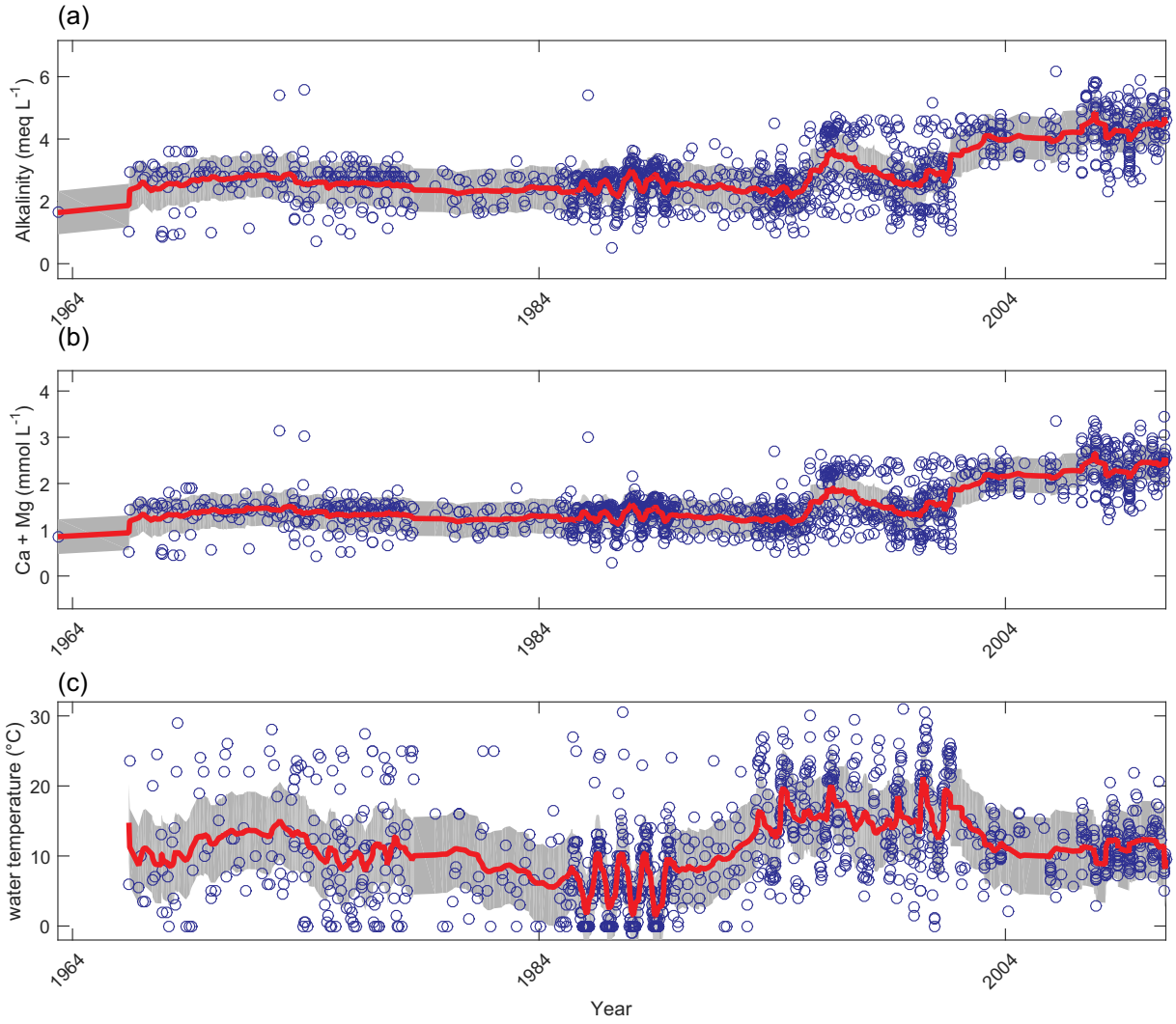

Fig. 10. Temporal variations of (a) Alkalinity, (b) Ca + Mg, and (c) water temperature of selected 1798 single measurements of GLORICH database. Blue circles represent each sample, red line is the smoothed function based on moving average, and, shaded region is the standard deviation of the smoothed function. Temporal data represents latitudes higher than 30°N due to lack of tropical samples (Fig. 1). (For interpretation of the references to colour in this figure legend, the reader is referred to the web version of this article.)

3.7. Seasonal changes

Several studies have demonstrated significant seasonal changes in river chemistry of carbonate rock dominated catchments, mainly due to temperature and discharge changes (Li et al. 2010; Liu et al. 2010; Liu et al. 2007; Roland et al. 2013; van Geldern et al. 2015; Zhang et al. 2012). The selected sample stations (Section 2.1) show a systematic preferential sampling time in March and September (Fig. 9a), and the mean and median alkalinity during these months is higher than during the other sampled months (Fig. 9b). Nevertheless, the mean alkalinity is slightly affected by this preferential sampling, from 3.2 meq L^{-1} to 3.0 meq L^{-1} when samples from March and September are excluded.

The shown underestimation of modelled alkalinity that is shown in the previous section, of approximately 1 meq L^{-1} in regions with temperature < 11 °C, suggests that the soil-rock PCO_2 function by Romero-Mujalli et al. (2018) presents a systematic bias of −1 meq L^{-1}. This bias might be influenced by seasonal changes and preferential sampling time of the springs used to calibrate the soil-rock PCO_2 function based on temperature and soil water content. However, seasonal changes could not be considered in the construction of Eq. (3), also due to the lack of temporal data for a large enough number of monitoring locations (Romero-Mujalli et al. 2018). Therefore, seasonality or other undiscovered causes may add to the observed systematic underestimation.

The sampling period of the selected 1798 samples from the GLORICH database ranges from May of 1963 until November of 2010. The temporal analysis shows an increase of alkalinity and Ca + Mg concentrations since at least 2001 (Fig. 10a and b, respectively). Temporal variation of water temperature (Fig. 10c) does not present a clear relationship with alkalinity or Ca + Mg concentrations besides seasonal changes during the late 1980s. In addition, the data filtering method implemented in this work reduces the input of evaporites, sulphides, silicates, and anthropogenic sources. Observed temporal variations of the chemical composition in the total dataset may reflect differences in soil-rock PCO_2, linked to variations in soil respiration. The soil-rock PCO_2 directly reflects the soil temperature and water content where the dissolution of calcite takes place and is not necessarily represented by water temperature of the river (Amundson and

Davidson 1990; Kuzyakov 2006; Mielnick and Dugas 2000; Romero-Mujalli et al. 2018).

4. Discussion

4.1. General discussion

Carbonate weathering rates and lateral river fluxes of the products depend on a combination of processes and system properties, which were tested for their relevance using hydrochemical information from catchments dominated by calcite dissolution, while focusing on alkalinity fluxes. The most prominent control in the critical zone is the soil-rock PCO_2, which is supplied by ecosystem respiration, which in turn depends on climate sensitive constraints like soil water content and temperature (Romero-Mujalli et al. 2018). The amount of CO_2 available for the dissolution process is in further controlled by the openness of the system. Semi-enclosed to closed system conditions reduce the weathering rate substantially. Further temperature dependent degassing of CO_2 from rivers (Lauerwald et al. 2015; van Geldern et al. 2015), also controlled by geomorphological properties, causes the average river water to be supersaturated with respect to calcite. The majority of investigated rivers have a saturation index with respect to calcite between 0.5 and 1, and alkalinity loss due precipitation of carbonates is observed in general (Calmels et al. 2014; Li et al. 2008; Liu et al. 2007), but difficult to constraint based on available global data. A rain event specific dilution parameterization maybe relevant for a global climate sensitive carbonate weathering representation, but its relevance and influence needs still to be worked out for the global scale. Simple phenomenological models based on average concentration-runoff relationships seem, for low runoff conditions, to properly address calcite weathering fluxes. However, rain event scale introduced variability cannot be replicated using the limited global datasets available. An enhanced global carbonate weathering model approach, therefore, should address at least the named processes, while parameterization of these processes for a spatially explicit global application demands further work and specifically more groundwater, spring water, and river water data along the lateral pathway of weathering product fluxes.

The presented results are based on selected data to represent idealized calcite catchments through minimizing the effect of sulphide oxidation, evaporite dissolution and dolomite contribution. The effects of these neglected minerals and related processes will be discussed below.

Two different approaches for soil PCO_2 estimates were considered in this work to constraint calcite dissolution rates, and both type of estimates present clear differences, mainly in deserts and polar regions (Romero-Mujalli et al. 2018). The function based on annual evapotranspiration (Eq. (2)) was developed using measurements of soil PCO_2 at different depth and during growing seasons for temperate areas, which causes elevated average soil PCO_2 representations in polar regions. On the other hand, the function based on land temperature and volumetric water content (Eq. (3)) is conceptually in concordance with ecosystem respiration models and it was created using spring water samples from catchments dominated by calcite dissolution.

The introduced approach calculating alkalinity concentrations based on a representative soil-rock-PCO_2 (*soil_tw_CO2*) for open system conditions allows to connect indirectly ecosystem respiration with calcite weathering fluxes. This work showed that for certain tropical areas, specifically such with deeper soil depth, > 1.3 m, a transition from open to semi- or even closed system conditions should be considered. However, concepts to address the locations where this happens, and how to represent this transition remain to be elaborated and depends on high quality soil maps. In addition, it was shown that the soil-rock PCO_2-representation demand further work to avoid underestimation of alkalinity fluxes (Fig. 8b) if the weathering fluxes should be constraint dynamically by a soil-rock-PCO_2 and not a simple river alkalinity parameterization based on temperature (Fig. 2). A coupling of carbonate weathering models with ecosystem models might be a further next step, if ecosystem respiration can be replicated properly. The analysis here suggests that evaluation of such coupled models need to include the soil properties and therefore a good representation of the soil-rock hydrology.

4.2. Equilibrium approach for calcite dissolution

The applied equilibrium model is constrained by a given PCO_2 and allows the calculation of major chemical species at equilibrium with the system $CaCO_3$-CO_2-H_2O for any given specific temperature. Therefore, the approach might be applied to calculate global calcite weathering from areas dominated by calcium carbonates for the present time and probably over time as it is sensitive to climate variables. However, carbonate rocks are rarely pure calcite. Dolomite ($CaMg(CO_3)_2$) dissolution has a different dissolution kinetics than calcite and the global pattern of river alkalinity in dependence of temperature changes with the Mg^{2+} concentration relative to Ca^{2+}. Higher alkalinity concentrations are observed in samples with relatively high Mg^{2+} content, in particular in some catchments with elevated temperatures (Fig. 2). This might be related to its influence on carbonate precipitation in rivers, because Mg^{2+} can inhibit or delay the precipitation of calcite minerals considering the saturation state of the water (Berner 1975; Bischoff 1968).

Some studies (Dreybrodt et al. 1996; Liu et al. 2005) have demonstrated that the dissolution of CO_2 in water represents the slowest rate of reaction in the open system $CaCO_3$-CO_2-H_2O. Therefore, it is feasible to consider that a soil-rock system is at equilibrium with calcite for open system conditions (Romero-Mujalli et al. 2018). This might represent an advantage over estimating a simplified soil PCO_2 function based on annual evapotranspiration (*soil_aet_CO2*).

Being less computationally expensive than chemical kinetic models, further improvements to constrain land to river weathering fluxes might result into incorporation into Earth system models (Goll et al. 2014). Because alkalinity is usually higher in groundwater than in surface waters due to degassing of CO_2 and precipitation of carbonates (Calmels et al. 2014; Li et al. 2008; Liu et al. 2007) further improvements in predicting mineral precipitation and CO_2 outgassing will allow to model sink terms during the transport.

4.3. Open and closed system conditions

Although studies related to spring water chemistry in karstic regions have found that the dissolution of carbonate minerals happens mainly under open to semi-open conditions with respect to soil PCO_2 (Calmels et al. 2014; Gillon et al. 2009; Romero-Mujalli et al. 2018; van Geldern et al. 2015), information from tropical regions where soils are usually more developed than in temperate regions is underrepresented. Nevertheless, for specific soil profiles, carbonate minerals are dissolved under closed system conditions with respect to soil PCO_2 (Deines et al. 1974; Faulkner 2006; Frisia et al. 2011; Thrailkill and Robl 1982).

The results obtained in this work showed that dissolution of calcite in soils might be developed under a gradual transition from fully open to closed system conditions because the kinetics of dissolution is fast enough to reach equilibrium with calcite before water infiltrates further into the soil profile, where soil production is limited. Soil depth seems not to be a good sole predictor for this transition, but a good one to determine, for a given setting, the start of the transition. A spatially-explicit description of the calcite weathering front, the depth of maximum calcite dissolution, combined with changes of soil CO_2 production with depth are required to constrain the transition of the system's condition of a catchment.

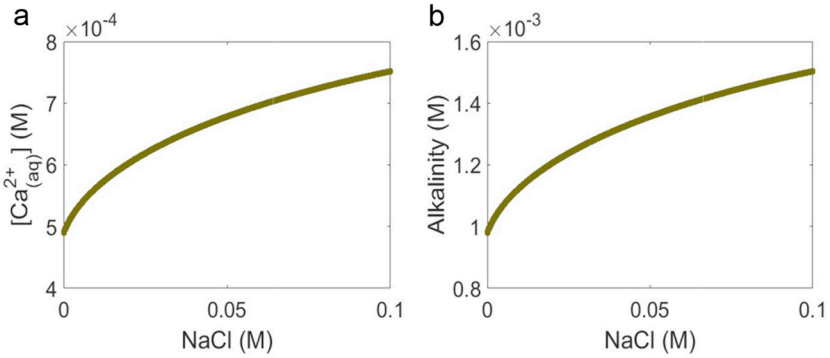

Fig. 11. Dependency of (a) Ca^{2+} (molar concentration) and (b) alkalinity (equivalent) on halite concentration for the open system NaCl-$CaCO_3$-CO_2-H_2O at 25 °C and PCO_2 of 0.000398 atm. Relationship as a result of Davies equation for activity coefficient (Eq. (A.12)).

4.4. Ideal calcite and real carbonate weathering system

In the present work, equilibrium calculations were developed to solve the ideal system $CaCO_3$-CO_2-H_2O, which allows to determine the chemical species due to calcite weathering. Nevertheless, in the natural system this is not often the case, instead, a complex system is more commonly found where water might be at equilibrium with other minerals, with consequences on the concentration of chemical species. Minerals commonly associated to carbonate lithologies are, e.g., evaporites and sulphides. These minerals produce different deviations from the ideal calcite equilibrium, increasing or decreasing concentrations of chemical species in the water.

Gypsum and anhydrite ($CaSO_4.2H_2O_{(s)}$ and $CaSO_{4(s)}$, respectively) are commonly found in evaporite containing lithologies and both show high solubility in water. A system at equilibrium composed of $CaCO_3$-CO_2-H_2O-gypsum/anhydrite would have approximately 40% less alkalinity if compared to the ideal calcite weathering system (Romero-Mujalli et al. 2018). However, the calcium ion (Ca^{2+}) concentration increases significantly, being able to reach 5 times the concentration presented in the ideal $CaCO_3$-CO_2-H_2O system. This is a consequence of the common ion effect produced by Ca^{2+}, which is shared between two chemical reactions, represented by Eq. (A.5) and the gypsum dissolution represented by the following chemical reaction:

$$CaSO_4x2H_2O_{(s)} \leftrightarrow Ca^{2+}_{(aq)} + SO^{2-}_{4(aq)} + 2H_2O_{(l)}, \quad (9)$$

Furthermore, evaporite minerals like halite ($NaCl_{(s)}$) or sylvite ($KCl_{(s)}$) differ from the effect of gypsum by controlling the ionic strength (I), thus the activity coefficients (Eq. (A.12)). Elevated contribution of dissolved NaCl to the water enhances calcite dissolution with reference to the ideal calcite weathering (by approximately 40–50% in the given example in Fig. 11).

Sulphide minerals are commonly found in sedimentary rocks and are easily oxidized in the soil profile (Calmels et al. 2007; Li et al. 2008), releasing sulphuric acid (H_2SO_4), a strong acid which may be neutralized by reactions with carbonates, as represented by the following chemical reaction:

$$2CaCO_{3(s)} + H_2SO_{4(aq)} \rightarrow 2Ca^{2+}_{(aq)} + SO^{2-}_{4(aq)} + 2HCO^{-}_{3(aq)}, \quad (10)$$

This reaction increases carbonate weathering significantly. However, the Ca^{2+}:Alkalinity molar ratio in this system can be 1:1, or even be lower. Therefore, calcite dissolution due to strong acids is not necessarily related to increasing alkalinity fluxes as compared to an ideal calcite dissolution, where the Ca^{2+}:Alkalinity ratio is 1:2. Sulphate ion concentration coming from pyrite oxidation might reach 0.5 mM (Calmels et al. 2007; Li et al. 2008). If comparing the concentration differences between the system $CaCO_3$-H_2O-CO_2-FeS_2-O_2 and the ideal carbonate dissolution ($CaCO_3$-H_2O-CO_2), due to the pyrite oxidation two different effects on Ca^{2+} and alkalinity can be expected. The Ca^{2+} concentration would be elevated by up to 20% if compared to the ideal calcite equilibrium calculation when reacting 0.267 mM of FeS_2 (Fig. 12a). Alkalinity, on the other hand, shows a decrease of approximately 5% with respect to the ideal calcite dissolution (Fig. 12b). In both cases, the decreasing trend with temperature follows the dissolution of pure calcite (Fig. 12).

Sedimentary carbonate rocks can contain a wide variety of different carbonate minerals, presenting each different dissolution kinetics and solubility. The range of Mg content in Ca-carbonates can vary significantly. Dolomite ($CaMg(CO_3)_2$), another common carbonate mineral, may influence calcite dissolution by adding Ca^{2+} and CO_3^{2-} to the solution (common ion effect). And although its dissolution is slower than calcite (Chou et al. 1989; Liu et al. 2005) and the calcite saturation state can be reached faster, the constant dissolution of dolomite can increase alkalinity in the solution and decrease Ca^{2+} while increasing Mg^{2+} to a Ca/Mg molar ratio closer to the one present in dolomite. We have tested a hypothetical example where the solution is at equilibrium with both minerals (calcite and dolomite saturation indices are 0) and

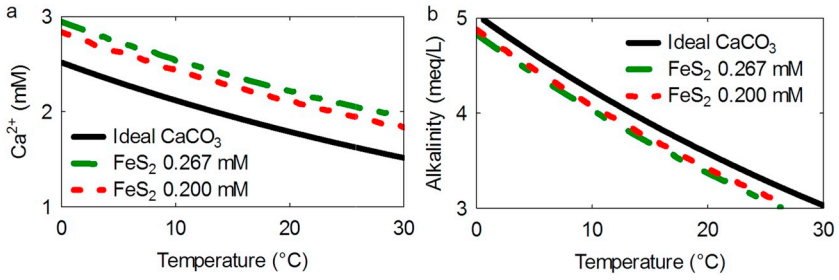

Fig. 12. Theoretical calculations of (a) Ca^{2+} concentration and (b) alkalinity against temperature. The black line represents the ideal carbonate equilibrium, the green dash line and red dash line stand for the system $CaCO_3$-H_2O-CO_2-O_2-FeS_2 with pyrite concentration of 0.267 mM and 0.200 mM, respectively. Results were obtained using the software PHREEQC with "wateq4f.dat" database (Parkhurst and Appelo 1999) considering a constant PCO_2 of 0.01 atm. (For interpretation of the references to colour in this figure legend, the reader is referred to the web version of this article.)

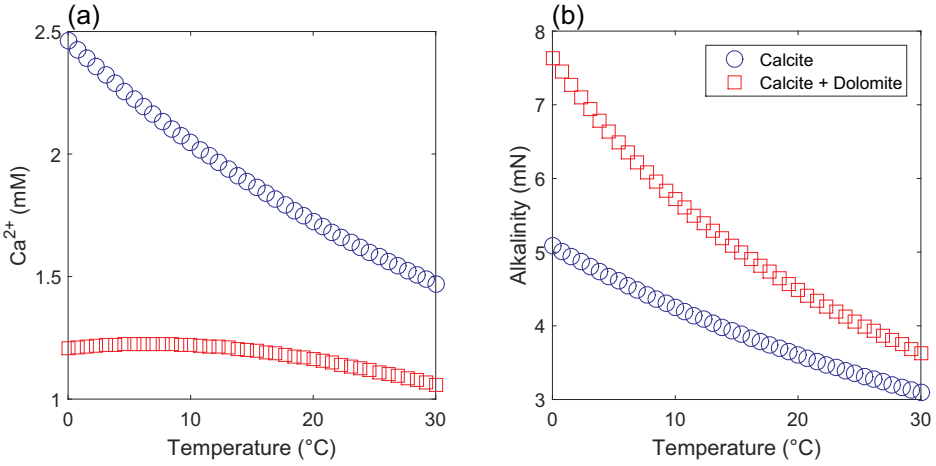

Fig. 13. Theoretical calculations of (a) Ca^{2+} concentration and (b) alkalinity against temperature. Blue circles represent the ideal carbonate equilibrium and red squares stand for the system $CaCO_3$-$CaMg(CO_3)_2$-CO_2-H_2O. Results were obtained using the software PHREEQC with "wateq4f.dat" database (Parkhurst and Appelo 1999) considering a constant PCO_2 of 0.01 atm. (For interpretation of the references to colour in this figure legend, the reader is referred to the web version of this article.)

Table 3
Ca^{2+} concentration and alkalinity deviations from the ideal system of carbonate dissolution due to different effects. The mean of deviations for the temperature range from 0 to 30 °C is given.

Effect	Deviation on Ca^{2+}	Deviation on alkalinity
Common ion effect (Gypsum)[a]	+400%	−40%
Ionic strength (NaCl)[b]	> +40%	> +40%
Strong acids (FeS_2 oxidation)[c]	+20%	~−5%
Dolomite ($CaMg(CO_3)_2$)[d]	~−40%	~+30%

[a] Gypsum Saturation index = 0; Calcite saturation index = 0 and; PCO_2 = 0.01 atm.
[b] NaCl = 0.1 M; Calcite saturation index = 0 and; PCO_2 = 0.000398 atm.
[c] FeS_2 = 0.267 M; Calcite saturation index = 0 and; PCO_2 = 0.01 atm.
[d] Dolomite saturation index = 0; Calcite saturation index = 0 and; PCO_2 = 0.01 atm.

solving the system using the software PHREEQC with "wateq4f.dat" database (Parkhurst and Appelo 1999). The results show that Ca^{2+} decreases with respect to a solution at equilibrium with only calcite by approximately 40% for the given temperature range in Fig. 13a. However, the behaviour of alkalinity is contrary, increasing up to 30% with respect to a solution without dolomite for the considered temperature range (Fig. 13b). Moreover, the dolomite effect is more complex than the results obtained by the hypothetical test because Mg^{2+} can enhance calcite dissolution rate under certain conditions (Ruiz-Agudo et al. 2009), and it might increase calcite solubility by increasing ionic strength.

The relatively low weathering rate of silicate minerals limits its impact on calcite dissolution. For instance, when weathering of anorthite is propitiated by carbonic acid, it can increase Ca^{2+} and alkalinity with a similar Ca^{2+}/alkalinity ratio than expected for pure calcite dissolution. However, the dissolution of calcite tends to decrease with temperature, while being opposite for silicate minerals, increasing with higher temperature.

In summary, three main different effects, the common ion effect, ionic strength change and reaction with strong acids need to be considered spatially explicitly to properly model the land-ocean alkalinity fluxes from a carbonate-dominated catchment. These effects show definite deviations from the ideal calcite dissolution system, summarized in Table 3. Ca^{2+} concentration presents a positive deviation for the three settings, highlighting the necessity to correct for these effects in order to consider equilibrium equations for ideal calcite dissolution. However, alkalinity behaves differently than Ca^{2+}; its concentration decreases in case sulphide and gypsum minerals are present in carbonate rocks, and it shows a directly proportional dependency on ionic strength.

4.5. Anthropogenic effects

Anthropogenic activity was identified to shift geochemical baselines of larger river systems over decades (Hartmann et al. 2007; Raymond and Hamilton 2018). Carbonate weathering system are due the fast dissolution kinetics very sensitive to anthropogenic influences (e.g. elevated levels of nitric acid or sulphur oxides). Li et al. (2008) have found that 40% of sulphuric acids in soils in Southwest China are related to anthropogenic activity. Furthermore, the use of fertilizers on soils may enhance carbonate weathering, for instance, the addition of N-fertilizers on soils may produce strong acids which can react with carbonate minerals and alter the carbon consumption (Perrin et al. 2008; Semhi et al. 2000) similar as the reaction through pyrite oxidation (Section 4.3). The application of fertilizers was found to decrease the contribution of soil CO_2 to riverine alkalinity by about 7–17% for studied catchments (Perrin et al. 2008). In addition, anthropogenic effects may control the precipitation rates of calcite in rivers due to phosphate inhibition (Bono et al. 2001; Dove and Hochella 1993; Zhang et al. 2012).

The use of karstic lands for agriculture or logging activities alters water quality, and changes the natural ecosystem functioning, which might cause an increase of soil degradation and erosion, e.g. due to an increase in surface runoff. The restoration of natural ecosystems on karst regions can take longer than for other land types (Milanović 2014; Urich 2002).

On the other hand, the addition of Ca and Mg carbonates (mainly calcite and dolomite) to soils, or liming, is a common agricultural practice to increase pH as well as Ca and Mg bioavailability (Diamond et al. 1992; Moreira and Fageria 2010). This activity can enhance, for areas other than karst regions, global carbonate weathering fluxes. The potential carbon sequestration due to agricultural liming has been estimated to be around 0.15×10^{12} mol C a^{-1} for soils located in United States of America (Hamilton et al. 2007). This is 3 to 4% of the global carbon fluxes from sedimentary carbonate rock areas calculated in this work with the idealized calcite weathering approach. However, this carbon sequestration potential depends also on the applied amount of fertilizers resulting in acid production, as discussed above.

ARTICLE IN PRESS

4.6. Future work for a more holistic carbonate weathering approach

Global CO_2 consumption due to calcite dissolution can be difficult to predict because temperature can exert different effects on the system $CaCO_3$-CO_2-H_2O. For instance, calcite can precipitate in the soil profile in warm and dry conditions, decreasing total weathering flux, as suggested by Goddéris et al. (2013). Moreover, the CO_2 evasion from rivers increases significantly with temperature (Lauerwald et al. 2015), and is one control on the calcite precipitation in the river bed, reducing the total carbon flux to the ocean. Locations and rates, where and at which saturation state this happens considering stream water velocity, biological activity, seasonality or street salt application (Dreybrodt et al. 1992; Rupp and Adams 1981; Suarez 1983; Szramek and Walter 2004; Zaihua et al. 1995), need to be determined for parameterization in a global model approach.

The function for alkalinity concentrations in dependence of land surface temperature is best representing the general dynamics of observed concentrations in rivers, but shows, based on the available data, large uncertainties. The approach could be enhanced by compiling more data, specifically from tropical regions, covering seasonality and in addition instant discharge information. An enhanced approach might include the identification of temperature depending alkalinity for different $[Ca^{2+}]$:$[Mg^{2+}]$ ratios (Fig. 2) and considering ranges of evaporite and sulphide contributions (among other characteristics like catchment size, steepness of the catchment, etc.). Tropical humid areas are of certain interest, due to the high contribution to global weathering fluxes, but also because there are still not enough constraints on the tropical settings (c.f. Fig. 8). However, it was shown that by coupling weathering and degassing processes with soil-rock properties, including a soil-rock PCO_2 constraint, a more holistic approach could be achieved in the future.

Thermodynamic equations can be implemented to estimate global CO_2 consumption due to carbonate weathering. However, the spatially-explicit mineralogical composition of carbonate systems is required to improve the presented idealized model. The different approaches presented in this work are able to assess the weathering of calcite composed carbonate sedimentary rocks (SC), and do not account for carbonate dissolution from other lithological classes, which contribute relevantly to global carbonate weathering fluxes (Hartmann et al. 2009; Hartmann et al. 2014b). Their contribution is needed to explain the high proportion of calculated global CO_2 consumption by carbonate weathering on the total global CO_2 consumption by weathering, using inverse methods (Gaillardet et al. 1999).

In a next step, the thermodynamic equation approach which is constrained by soil PCO_2 due to biological activity should be coupled with a degassing model without increasing significantly computational time for calculations. In the future, detailed models should be created to quantify the global effect of CO_2 evasion from rivers, while considering the transitional zone from open to closed conditions in the soil-rock-system. In addition, the dilution effect due to rain events for different land cover and geomorphological setups, further mineral phases and, finally, the effect of anthropogenic activity need to be addressed. Latter processes might be relevant in order to understand to what degree human activity influences the lateral alkalinity fluxes and to quantify the response to climate processes.

5. Conclusion

The findings support that calcite weathering fluxes in the soil-rock profile are higher than the land-ocean flux via river systems. The identified climate sensitivity of carbonate weathering suggests that an increase of the mean land temperature is not necessarily causing an increase of lateral weathering fluxes. In addition, increasing temperatures have the potential to increase precipitation of carbonate minerals due to its influence on the carbonate system, as suggested, for example, by Goddéris et al. (2013).

The observed temperature dependency of alkalinity in rivers suggests that calcite dissolution increases with temperature in cold to temperate regions up to a maximum around 11 °C for land surface temperature. This is in part because of an increase in soil-rock PCO_2. The opposite is the case for warmer regions, despite of the identified higher levels of soil-rock PCO_2. However, a general impact of climate change on global calcite dissolution rates is difficult to identify, due to discussed further factors, the abundance of other minerals, locations of non-open system conditions, anthropogenic influences, possible dilution due to relevant surface runoff contribution to the river water, and the CO_2 evasion from surface waters. Hence, to be able to model global carbonate rock weathering, instead of the idealized system presented here, would demand that these processes be addressed. However, for most of these processes there is still an insufficient amount of field studies available to parameterize all of these effects and to address the geochemical variety of carbonate rock systems. Therefore, modelling carbonate weathering at the global scale and estimating the impact of climate change will rely, until solved, on idealized weathering models, being either conceptual or mechanistic in high detail.

Future works should focus on understanding the global effect of instream processes in the carbon cycle and the predominance of closed to semi-closed conditions with respect to CO_2 availability for carbonate weathering. For this, more temporal river chemistry data should be collected, mainly in tropical karst regions, to decipher the main mechanism causing the decrease in alkalinity concentration observed in river data.

Acknowledgments

Funding for this work has been provided by German Research Foundation (DFG) through the Cluster of Excellence CLISAP2 (DFG Exec177, Universität Hamburg), and BMBF-project PALMOD (Ref 01LP1506C) through the German Ministry of Education and Science (BMBF) as Research for Sustainability initiative (FONA).

Appendix A. Equilibrium model

The concentration of chemical species at equilibrium with calcite dissolution was calculated considering open conditions for the system $CaCO_3$-H_2O-CO_2 and a given calcite saturation index (SIc = 0 or SIc = 0.5, when applicable), represented by the following chemical reactions:

$$2H_2O_{(l)} \leftrightarrow H_3O^+_{(aq)} + OH^-_{(aq)}, \quad (A.1)$$

$$CO_{2(g)} \leftrightarrow CO_{2(aq)}, \quad (A.2)$$

ARTICLE IN PRESS

$$CO_{2(aq)} + 2H_2O_{(l)} \leftrightarrow HCO_{3(aq)}^{-} + H_3O_{(aq)}^{+}, \quad (A.3)$$

$$HCO_{3(aq)}^{-} + H_2O_{(l)} \leftrightarrow CO_{3(aq)}^{2-} + H_3O_{(aq)}^{+}, \quad (A.4)$$

$$CaCO_{3(s)} \leftrightarrow Ca_{(aq)}^{2+} + CO_{3(aq)}^{2-}, \quad (A.5)$$

with equilibrium constants K_w, K_{PCO2}, K_1, K_{a2} and K_{sp}, expressed as:

$$K_w = (H_3O^+)\,(OH^-), \quad (A.6)$$

$$K_{PCO_2} = \frac{(CO_{2(aq)})}{fCO_2}, \quad (A.7)$$

$$K_1 = \frac{(HCO_3^-)(H_3O^+)}{(CO_{2(aq)})}, \quad (A.8)$$

$$K_{a2} = \frac{(CO_3^{2-})(H_3O^+)}{(HCO_3^-)}, \quad (A.9)$$

$$K_{sp} = (Ca^{2+})\,(CO_3^{2-}), \quad (A.10)$$

where parenthesis indicates activity of chemical species and "f" fugacity of gases. In this work we assumed that fugacity is equal to partial pressure. Alkalinity was assumed to be $[HCO_3^-] + 2[CO_3^{2-}] + [OH^-] - [H^+]$. The equilibrium equations were solved using the charge balance equation and the Newton-Raphson method for the numerical approach. The standard equilibrium constants (K) at 25 °C for each chemical equation (from Eqs. (A.1) to (A.5)) are reported in Table A.1, the temperature dependency of the equilibrium constants (K) and the Henry's constant (K_{PCO2}) was calculated using the Van't Hoff equation (Eq. (A.11)), given by:

$$ln\left(\frac{K_2}{K_1}\right) = -\frac{\Delta H^\circ}{R}\left(\frac{1}{T_2} - \frac{1}{T_1}\right), \quad (A.11)$$

where T represents the absolute temperature in Kelvin, ΔH° is the standard enthalpy of reaction and R is the gas constant. Furthermore, the activity coefficient of each chemical species i (γ_i) was calculated using the Davies Equation (Eq. (A.12)):

$$log\,\gamma_i = -Az_i^2\left(\frac{\sqrt{I}}{1+\sqrt{I}} - 0.3I\right), \quad (A.12)$$

where A is a temperature related constant, z_i is the charge of the chemical species and I is the ionic strength of the solution.

Table A.1
Solubility product constants at 25 °C (K) and standard enthalpy (ΔH°) for the reactions considered in this work (Romero-Mujalli et al. 2018).

Reaction number	Constant (K)	ΔH_r° (KJ/mol)
A.1	10^{-14}	55.9066
A.2	$10^{-1.468}$[a]	−19.983
A.3	$10^{-6.352}$	9.109
A.4	$10^{-10.329}$	14.90
A.5	$10^{-8.48}$	−9.61

Thermodynamic data was taken from phreeqc.dat database after Parkhurst and Appelo (1999).
[a] Henry's constant for dissolution of gas CO_2 in water.

Furthermore, closed system conditions were calculated using a simplified equation based on the following summarized chemical equation for calcite dissolution:

$$CaCO_{3(s)} + CO_{2(aq)} + H_2O_{(l)} \leftrightarrow Ca_{(aq)}^{2+} + 2HCO_{3(aq)}^{-}, \quad (A.13)$$

The total concentration of calcium ions, $[Ca^{2+}]_t$ was assumed to be equal to half of the concentration of carbonate acid, $[HCO_3^-]$. In order to account for closed system conditions, the initial PCO_2 (PCO_{2i}) should be equal to $[Ca^{2+}]_t + [CO_{2(aq)}]$, and $[Ca^{2+}]_t$ is determined by solving the following equation:

$$[Ca^{2+}]_t^3 + \frac{K_{sp}K_1}{4K_{a2}\gamma_1^2\gamma_2}[Ca^{2+}]_t - \frac{K_{sp}K_1K_{PCO_2}}{4K_{a2}\gamma_1^2\gamma_2}PCO_{2i} = 0, \quad (A.14)$$

where γ_z stands for the activity coefficient for ions of charge "z" (Eq. (A.12)), and K_{sp}, K_1, K_{a2}, K_{PCO2} are the equilibrium constants for Eqs. (A.5), (A.3), (A.4), and (A.2), respectively (see Table A.1).

ARTICLE IN PRESS

Appendix B. Schematic of global calcite weathering model

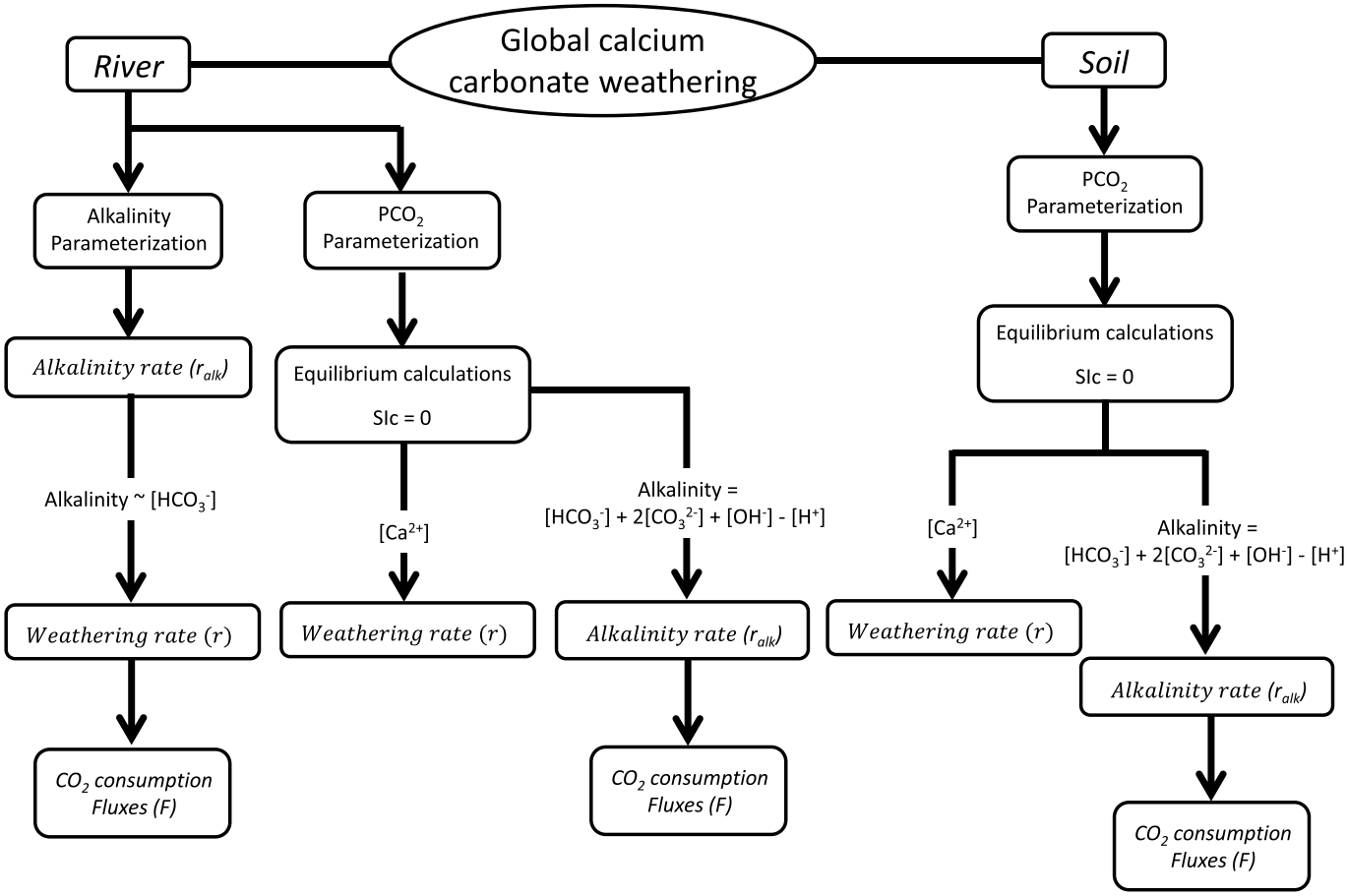

Fig. B.1. Schematic of how calcium carbonate dissolution was modelled using different constraints. The assumption alkalinity is approximately $[HCO_3^-]$ was applied for the alkalinity parameterization only to calculate global alkalinity rates, equivalent to the weathering rate (r). The equilibrium approaches were used to calculate concentrations of Ca and alkalinity due to dissolution of calcite. For this scenario, alkalinity is represented as $[HCO_3^-] + 2[CO_3^{2-}] + [OH^-] - [H^+]$. Alkalinity weathering rates (r) and resulting CO_2 fluxes are discussed in the main text.

References

Amiotte-Suchet, P., Probst, J.-L., 1993. Modelling of atmospheric CO 2 consumption by chemical weathering of rocks: application to the Garonne, Congo and Amazon basins. Chem. Geol. 107 (3), 205–210.

Amiotte-Suchet, P., Probst, J.-L., 1995. A global model for present-day atmospheric/soil CO2 consumption by chemical erosion of continental rocks (GEM-CO2). Tellus Ser. B Chem. Phys. Meteorol. 47 (1–2), 273–280.

Amundson, R.G., Davidson, E.A., 1990. Carbon dioxide and nitrogenous gases in the soil atmosphere. J. Geochem. Explor. 38 (1–2), 13–41.

Arvidson, R.S., Mackenzie, F.T., Guidry, M., 2006. MAGic: a Phanerozoic model for the geochemical cycling of major rock-forming components. Am. J. Sci. 306 (3), 135–190.

Batjes, N., 2005. ISRIC-WISE Global Data Set of Derived Soil Properties on a 0.5 by 0.5 Degree Grid (Version 3.0). ISRIC-World Soil Information, Wageningen.

Beaulieu, E., Goddéris, Y., Labat, D., Roelandt, C., Calmels, D., Gaillardet, J., 2011. Modeling of water-rock interaction in the Mackenzie basin: competition between sulfuric and carbonic acids. Chem. Geol. 289 (1–2), 114–123.

Beaulieu, E., Goddéris, Y., Donnadieu, Y., Labat, D., Roelandt, C., 2012. High sensitivity of the continental-weathering carbon dioxide sink to future climate change. Nat. Clim. Chang. 2 (5), 346–349.

Berner, R., 1975. The role of magnesium in the crystal growth of calcite and aragonite from sea water. Geochim. Cosmochim. Acta 39 (4) (489IN3495-494504).

Berner, E.K., Berner, R.A., 2012. Global Environment: Water, Air, and Geochemical Cycles. Princeton University Press.

Berner, R.A., Lasaga, A.C., Garrels, R.M., 1983. The carbonate-silicate geochemical cycle and its effect on atmospheric carbon dioxide over the past 100 million years. Am. J. Sci. 283, 641–683.

Bischoff, J.L., 1968. Kinetics of calcite nucleation: magnesium ion inhibition and ionic strength catalysis. J. Geophys. Res. 73 (10), 3315–3322.

Bluth, G.J., Kump, L.R., 1994. Lithologic and climatologic controls of river chemistry. Geochim. Cosmochim. Acta 58 (10), 2341–2359.

Bono, P., Dreybrodt, W., Ercole, S., Percopo, C., Vosbeck, K., 2001. Inorganic calcite precipitation in Tartare karstic spring (Lazio, central Italy): field measurements and theoretical prediction on depositional rates. Environ. Geol. 41 (3–4), 305–313.

Brook, G.A., Folkoff, M.E., Box, E.O., 1983. A world model of soil carbon dioxide. Earth Surf. Process. Landf. 8 (1), 79–88.

Calmels, D., Gaillardet, J., Brenot, A., France-Lanord, C., 2007. Sustained sulfide oxidation by physical erosion processes in the Mackenzie River basin: climatic perspectives. Geology 35 (11), 1003.

Calmels, D., Gaillardet, J., François, L., 2014. Sensitivity of carbonate weathering to soil CO2 production by biological activity along a temperate climate transect. Chem. Geol. 390, 74–86.

Chou, L., Garrels, R.M., Wollast, R., 1989. Comparative study of the kinetics and mechanisms of dissolution of carbonate minerals. Chem. Geol. 78 (3–4), 269–282.

Deines, P., Langmuir, D., Harmon, R.S., 1974. Stable carbon isotope ratios and the existence of a gas phase in the evolution of carbonate ground waters. Geochim. Cosmochim. Acta 38 (7), 1147–1164.

Diamond, M., Hirst, D., Winder, L., Crawshaw, D.H., Prigg, R.F., 1992. The effect of liming agricultural land on the chemistry and biology of the River Esk, north-west England. Environ. Pollut. 78 (1–3), 179–185.

Dove, P.M., Hochella, M.F., 1993. Calcite precipitation mechanisms and inhibition by orthophosphate: in situ observations by scanning force microscopy. Geochim. Cosmochim. Acta 57 (3), 705–714.

Dreybrodt, W., Buhmann, D., Michaelis, J., Usdowski, E., 1992. Geochemically controlled calcite precipitation by CO2 outgassing: field measurements of precipitation rates in comparison to theoretical predictions. Chem. Geol. 97 (3–4), 285–294.

Dreybrodt, W., Lauckner, J., Zaihua, L., Svensson, U., Buhmann, D., 1996. The kinetics of the reaction CO 2+ H 2 O→H+ + HCO 3− as one of the rate limiting steps for the dissolution of calcite in the system H 2 O·CO 2·CaCO 3. Geochim. Cosmochim. Acta 60 (18), 3375–3381.

Dupré, B., Dessert, C., Oliva, P., Goddéris, Y., Viers, J., François, L., Millot, R., Gaillardet, J., 2003. Rivers, chemical weathering and Earth's climate. Compt. Rendus Geosci.

335 (16), 1141–1160.
Dürr, H.H., Meybeck, M., Dürr, S.H., 2005. Lithologic composition of the Earth's continental surfaces derived from a new digital map emphasizing riverine material transfer. Glob. Biogeochem. Cycles 19 (4) (n/a-n/a).
Edwards, C., Reichle, D., Crossley Jr., D., 1973. The role of soil invertebrates in turnover of organic matter and nutrients. In: Analysis of Temperate Forest Ecosystems. Springer, pp. 147–172.
Egli, M., Mirabella, A., Sartori, G., 2008. The role of climate and vegetation in weathering and clay mineral formation in late Quaternary soils of the Swiss and Italian Alps. Geomorphology 102 (3–4), 307–324.
Faulkner, T., 2006. Limestone dissolution in phreatic conditions at maximum rates and in pure, cold, water. Cave and Karst Sci. 33 (1), 11.
Fekete, B.M., Vörösmarty, C.J., Grabs, W., 2002. High-resolution fields of global runoff combining observed river discharge and simulated water balances. Glob. Biogeochem. Cycles 16 (3) (15-1-15-10).
Frisia, S., Fairchild, I.J., Fohlmeister, J., Miorandi, R., Spötl, C., Borsato, A., 2011. Carbon mass-balance modelling and carbon isotope exchange processes in dynamic caves. Geochim. Cosmochim. Acta 75 (2), 380–400.
Gaillardet, J., Dupré, B., Louvat, P., Allegre, C., 1999. Global silicate weathering and CO 2 consumption rates deduced from the chemistry of large rivers. Chem. Geol. 159 (1), 3–30.
Gaillardet, J., Calmels, D., Romero-Mujalli, G., Sakarova, E., Hartmann, J., 2018. Global climate control on carbonate weathering intensity. Chem. Geol. https://doi.org/10.1016/j.chemgeo.2018.05.009.
Gillon, M., Barbecot, F., Gibert, E., Alvarado, J.C., Marlin, C., Massault, M., 2009. Open to closed system transition traced through the TDIC isotopic signature at the aquifer recharge stage, implications for groundwater 14C dating. Geochim. Cosmochim. Acta 73 (21), 6488–6501.
Goddéris, Y., François, L.M., Probst, A., Schott, J., Moncoulon, D., Labat, D., Viville, D., 2006. Modelling weathering processes at the catchment scale: the WITCH numerical model. Geochim. Cosmochim. Acta 70 (5), 1128–1147.
Goddéris, Y., Brantley, S.L., François, L.M., Schott, J., Pollard, D., Déqué, M., Dury, M., 2013. Rates of consumption of atmospheric CO2 through the weathering of loess during the next 100 yr of climate change. Biogeosciences 10 (1), 135–148.
Goll, D.S., Moosdorf, N., Hartmann, J., Brovkin, V., 2014. Climate-driven changes in chemical weathering and associated phosphorus release since 1850: implications for the land carbon balance. Geophys. Res. Lett. 41 (10), 3553–3558.
Gombert, P., 2002. Role of karstic dissolution in global carbon cycle. Glob. Planet. Chang. 33 (1), 177–184.
Hamilton, S.K., Kurzman, A.L., Arango, C., Jin, L., Robertson, G.P., 2007. Evidence for carbon sequestration by agricultural liming. Glob. Biogeochem. Cycles 21 (2).
Hartmann, J., Moosdorf, N., 2012. The new global lithological map database GLiM: a representation of rock properties at the Earth surface. Geochem. Geophys. Geosyst. 13 (12) (n/a-n/a).
Hartmann, J., Jansen, N., Kempe, S., Dürr, H.H., 2007. Geochemistry of the river Rhine and the upper Danube: recent trends and lithological influence on baselines. J. Environ. Sci. Sustain. Soc. 1, 39–46.
Hartmann, J., Jansen, N., Dürr, H.H., Kempe, S., Köhler, P., 2009. Global CO2-consumption by chemical weathering: what is the contribution of highly active weathering regions? Glob. Planet. Chang. 69 (4), 185–194.
Hartmann, J., Dürr, H.H., Moosdorf, N., Meybeck, M., Kempe, S., 2012. The geochemical composition of the terrestrial surface (without soils) and comparison with the upper continental crust. Int. J. Earth Sci. 101 (1), 365–376.
Hartmann, J., Lauerwald, R., Moosdorf, N., 2014a. A Brief Overview of the GLObal RIver Chemistry Database, GLORICH. Procedia Earth Planet. Sci. 10, 23–27.
Hartmann, J., Moosdorf, N., Lauerwald, R., Hinderer, M., West, A.J., 2014b. Global chemical weathering and associated P-release — the role of lithology, temperature and soil properties. Chem. Geol. 363, 145–163.
Hercod, D.J., Brady, P.V., Gregory, R.T., 1998. Catchment-scale coupling between pyrite oxidation and calcite weathering. Chem. Geol. 151 (1), 259–276.
Hijmans, R.J., Cameron, S.E., Parra, J.L., Jones, P.G., Jarvis, A., 2005. Very high resolution interpolated climate surfaces for global land areas. Int. J. Climatol. 25 (15), 1965–1978.
Kempe, S., 1979a. Carbon in the freshwater cycle. In: Bolin, B., Degens, E.T., Kempe, S., Ketner, P. (Eds.), The Global Carbon Cycle: Scope 13. Unwin Brothers Ltd., New York, pp. 317–342.
Kempe, S., 1979b. Carbon in the rock cycle. In: Bolin, B., Degens, E.T., Kempe, S., Ketner, P. (Eds.), The Global Carbon Cycle: SCOPE 13. John Wiley and Sons, New York, pp. 333–375.
Kuzyakov, Y., 2006. Sources of CO2 efflux from soil and review of partitioning methods. Soil Biol. Biochem. 38 (3), 425–448.
Lauerwald, R., Laruelle, G.G., Hartmann, J., Ciais, P., Regnier, P.A., 2015. Spatial patterns in CO2 evasion from the global river network. Glob. Biogeochem. Cycles 29 (5), 534–554.
Li, S.-L., Calmels, D., Han, G., Gaillardet, J., Liu, C.-Q., 2008. Sulfuric acid as an agent of carbonate weathering constrained by δ13CDIC: examples from Southwest China. Earth Planet. Sci. Lett. 270 (3–4), 189–199.
Li, S.-L., Liu, C.-Q., Li, J., Lang, Y.-C., Ding, H., Li, L., 2010. Geochemistry of dissolved inorganic carbon and carbonate weathering in a small typical karstic catchment of Southwest China: isotopic and chemical constraints. Chem. Geol. 277 (3–4), 301–309.
Liu, Z., Yuan, D., Dreybrodt, W., 2005. Comparative study of dissolution rate-determining mechanisms of limestone and dolomite. Environ. Geol. 49 (2), 274–279.
Liu, Z., Li, Q., Sun, H., Wang, J., 2007. Seasonal, diurnal and storm-scale hydrochemical variations of typical epikarst springs in subtropical karst areas of SW China: soil CO2 and dilution effects. J. Hydrol. 337 (1–2), 207–223.
Liu, Z., Dreybrodt, W., Wang, H., 2010. A new direction in effective accounting for the atmospheric CO2 budget: considering the combined action of carbonate dissolution, the global water cycle and photosynthetic uptake of DIC by aquatic organisms. Earth Sci. Rev. 99 (3–4), 162–172.
Mackenzie, F.T., Garrels, R.M., 1966. Chemical mass balance between rivers and oceans. Am. J. Sci. 264 (7), 507–525.
Martens, B., Miralles, D.G., Lievens, H., van der Schalie, R., de Jeu, R.A., Fernández-Prieto, D., Beck, H.E., Dorigo, W.A., Verhoest, N.E., 2016. GLEAM v3: satellite-based land evaporation and root-zone soil moisture. Geosci. Model Dev. 10, 1903–1925. https://doi.org/10.5194/gmd-10-1903-2017.
Martin, J.B., 2017. Carbonate minerals in the global carbon cycle. Chem. Geol. 449, 58–72.
Marx, A., Dusek, J., Jankovec, J., Sanda, M., Vogel, T., Geldern, R., Hartmann, J., Barth, J., 2017. A review of CO2 and associated carbon dynamics in headwater streams: a global perspective. Rev. Geophys. 55, 560–585.
Meybeck, M., 1987. Global chemical weathering of surficial rocks estimated from river dissolved loads. Am. J. Sci. 287 (5), 401–428.
Mielnick, P., Dugas, W.A., 2000. Soil CO2 flux in a tallgrass prairie. Soil Biol. Biochem. 32 (2), 221–228.
Milanović, P., 2014. Hydraulic properties of karst groundwater and its impacts on large structures. In: H2Karst Research in Limestone Hydrogeology. Springer, pp. 19–48.
Miralles, D., Holmes, T., De Jeu, R., Gash, J., Meesters, A., Dolman, A., 2011. Global land-surface evaporation estimated from satellite-based observations. Hydrol. Earth Syst. Sci. 15 (2), 453.
Moosdorf, N., Hartmann, J., Lauerwald, R., Hagedorn, B., Kempe, S., 2011. Atmospheric CO2 consumption by chemical weathering in North America. Geochim. Cosmochim. Acta 75 (24), 7829–7854.
Moreira, A., Fageria, N.K., 2010. Liming influence on soil chemical properties, nutritional status and yield of alfalfa grown in acid soil. Rev. Bras. Ciênc. Solo 34 (4), 1231–1239.
Norton, K.P., Molnar, P., Schlunegger, F., 2014. The role of climate-driven chemical weathering on soil production. Geomorphology 204, 510–517.
Parkhurst, D.L., Appelo, C., 1999. User's Guide to PHREEQC (Version 2): A Computer Program for Speciation, Batch-Reaction, One-Dimensional Transport, and Inverse Geochemical Calculations.
Perrin, A.-S., Probst, A., Probst, J.-L., 2008. Impact of nitrogenous fertilizers on carbonate dissolution in small agricultural catchments: Implications for weathering CO2 uptake at regional and global scales. Geochim. Cosmochim. Acta 72 (13), 3105–3123.
Pu, T., He, Y., Zhang, T., Wu, J., Zhu, G., Chang, L., 2013. Isotopic and geochemical evolution of ground and river waters in a karst dominated geological setting: a case study from Lijiang basin, South-Asia monsoon region. Appl. Geochem. 33, 199–212.
Raymond, P.A., Hamilton, S.K., 2018. Anthropogenic influences on riverine fluxes of dissolved inorganic carbon to the oceans. Limnol. Oceanogr. Lett. 3 (3), 143–155.
Reddy, M.M., Plummer, L.N., Busenberg, E., 1981. Crystal growth of calcite from calcium bicarbonate solutions at constant P CO2 and 25 °C: a test of a calcite dissolution model. Geochim. Cosmochim. Acta 45 (8), 1281–1289.
Roelandt, C., Goddéris, Y., Bonnet, M.P., Sondag, F., 2010. Coupled modeling of biospheric and chemical weathering processes at the continental scale. Glob. Biogeochem. Cycles 24 (2) (n/a-n/a).
Roland, M., Serrano-Ortiz, P., Kowalski, A.S., Goddéris, Y., Sánchez-Cañete, E.P., Ciais, P., Domingo, F., Cuezva, S., Sanchez-Moral, S., Longdoz, B., Yakir, D., Van Grieken, R., Schott, J., Cardell, C., Janssens, I.A., 2013. Atmospheric turbulence triggers pronounced diel pattern in karst carbonate geochemistry. Biogeosciences 10 (7), 5009–5017.
Romero-Mujalli, G., Hartmann, J., Börker, J., Gaillardet, J., Calmels, D., 2018. Ecosystem controlled soil-rock pCO2 and carbonate weathering – constraints by temperature and soil water content. Chem. Geol. https://doi.org/10.1016/j.chemgeo.2018.01.030.
Ruiz-Agudo, E., Putnis, C., Jiménez-López, C., Rodriguez-Navarro, C., 2009. An atomic force microscopy study of calcite dissolution in saline solutions: the role of magnesium ions. Geochim. Cosmochim. Acta 73 (11), 3201–3217.
Rupp, G.L., Adams, V.D., 1981. Calcium Carbonate Precipitation as Influenced by Stream Primary Production.
Semhi, K., Amiotte-Suchet, P., Clauer, N., Probst, J.-L., 2000. Impact of nitrogen fertilizers on the natural weathering-erosion processes and fluvial transport in the Garonne basin. Appl. Geochem. 15 (6), 865–878.
Serrano-Ortiz, P., Roland, M., Sanchez-Moral, S., Janssens, I.A., Domingo, F., Goddéris, Y., Kowalski, A.S., 2010. Hidden, abiotic CO2 flows and gaseous reservoirs in the terrestrial carbon cycle: review and perspectives. Agric. For. Meteorol. 150 (3), 321–329.
Spence, J., Telmer, K., 2005. The role of sulfur in chemical weathering and atmospheric CO2 fluxes: evidence from major ions, δ13CDIC, and δ34SSO4 in rivers of the Canadian Cordillera. Geochim. Cosmochim. Acta 69 (23), 5441–5458.
Suarez, D., 1983. Calcite supersaturation and precipitation kinetics in the Lower Colorado River, All-American Canal and East Highline Canal. Water Resour. Res. 19 (3), 653–661.
Szramek, K., Walter, L.M., 2004. Impact of carbonate precipitation on riverine inorganic carbon mass transport from a mid-continent, forested watershed. Aquat. Geochem. 10 (1–2), 99–137.
Thrailkill, J., Robl, T.L., 1982. Carbonate geochemistry of vadose water recharging limestone aquifers. In: Developments in Water Science. Elsevier, pp. 195–208.
Torres, M.A., Moosdorf, N., Hartmann, J., Adkins, J.F., West, A.J., 2017. Glacial weathering, sulfide oxidation, and global carbon cycle feedbacks. Proc. Natl. Acad. Sci. 114 (33), 8716–8721.
Urich, P.B., 2002. Land Use in Karst Terrain: Review of Impacts of Primary Activities on Temperate Karst Ecosystems. Department of Conservation Wellington.

ARTICLE IN PRESS

van Geldern, R., Schulte, P., Mader, M., Baier, A., Barth, J.A.C., 2015. Spatial and temporal variations ofpCO2, dissolved inorganic carbon and stable isotopes along a temperate karstic watercourse. Hydrol. Process. 29 (15), 3423–3440.

Walker, J.C.G., Hays, P.B., Kasting, J.F., 1981. A negative feedback mechanism for the long-term stabilization of Earth's surface temperature. J. Geophys. Res. 86 (C10), 9776.

Wang, S., Yeager, K.M., Wan, G., Liu, C.-Q., Liu, F., Lü, Y., 2015. Dynamics of CO2 in a karst catchment in the southwestern plateau, China. Environ. Earth Sci. 73 (5), 2415–2427.

White, A.F., Blum, A.E., 1995. Effects of climate on chemical_ weathering in watersheds. Geochim. Cosmochim. Acta 59 (9), 1729–1747.

Zaihua, L., Svensson, U., Dreybrodt, W., Daoxian, Y., Buhmann, D., 1995. Hydrodynamic control of inorganic calcite precipitation in Huanglong Ravine, China: field measurements and theoretical prediction of deposition rates. Geochim. Cosmochim. Acta 59 (15), 3087–3097.

Zhang, J., Wang, H., Liu, Z., An, D., Dreybrodt, W., 2012. Spatial–temporal variations of travertine deposition rates and their controlling factors in Huanglong Ravine, China – a world's heritage site. Appl. Geochem. 27 (1), 211–222.

Zhong, J., Li, S.-l., Tao, F., Yue, F., Liu, C.-Q., 2017. Sensitivity of chemical weathering and dissolved carbon dynamics to hydrological conditions in a typical karst river. Sci. Rep. 7.